AGU PUBLICATIONS

Geochemistry, Geophysics, Geosystems

RESEARCH ARTICLE
10.1002/2015GC005822

Key Points:
- Ba/Ca analyses of *G. ruber* from the central Bay of Bengal for 70–40 ka
- A freshwater stack for the last 80 ka is presented, validated by these data
- The processes modulating Indian monsoon freshwater flux were identified

Supporting Information:
- Supporting Information S1
- Data Set S1

Correspondence to:
D. Evans,
d.evans@yale.edu

Citation:
Evans, D., R. Bhatia, H. Stoll, and W. Müller (2015), LA-ICPMS Ba/Ca analyses of planktic foraminifera from the Bay of Bengal: Implications for late Pleistocene orbital control on monsoon freshwater flux, *Geochem. Geophys. Geosyst.*, *16*, 2598–2618, doi:10.1002/2015GC005822.

Received 18 MAR 2015
Accepted 11 JUL 2015
Accepted article online 16 JUL 2015
Published online 18 AUG 2015

LA-ICPMS Ba/Ca analyses of planktic foraminifera from the Bay of Bengal: Implications for late Pleistocene orbital control on monsoon freshwater flux

David Evans[1,2], Rehemat Bhatia[1,3], Heather Stoll[4], and Wolfgang Müller[1]

[1]Department of Earth Sciences, Royal Holloway University of London, London, UK, [2]Now at Department of Geology and Geophysics, Yale University, New Haven, Connecticut, USA, [3]Now at Department of Earth Sciences, University College London, London, UK, [4]Department of Geology, University of Oviedo, Oviedo, Asturias, Spain

Abstract Indian Summer Monsoon (ISM) indices are characterized by large secular variation during both glacials and interglacials. Although much information about palaeomonsoon intensity is derived from such indicies, current data sets do not relate simply to precipitation. In order to directly constrain the variability of ISM freshwater flux to the Bay of Bengal, we report Ba/Ca LA-ICPMS data of the surface-dwelling foraminifera *Globigerinoides ruber* from core RC12–343 (central Bay of Bengal) between 68 and 47 ka. Planktic foraminifera Ba/Ca directly relates to seawater Ba/Ca, in turn principally controlled by freshwater flux. Our foraminifera-derived Ba/Ca_{sw} record for the central Bay of Bengal is highly coherent with that derived from $\delta^{18}O$ measurements of the same material, implying that these reconstructions are not significantly biased by potential shifts in $\delta^{18}O_{freshwater}$. Validating this method allows us to produce a freshwater stack for the last 80 ka for the Bay of Bengal, enabling the orbital controls on ISM precipitation to be examined for the first time. The highest freshwater flux in the last 80 ka was ~3X larger than present and occurred during the early-mid Holocene. We show that the orbital timing of this record is best explained by a combination of factors with a weighting of ~45% given to the 30°N-equator mean summer insolation gradient and ~55% given to the variability of May–July insolation at the equator and June–July insolation at 30°N. These processes are consistent with current mechanistic understanding of ISM forcings and demonstrate a dominant orbital control on monsoon precipitation amount on millennial timescales.

1. Introduction

The most prominent expression of the Indian Summer Monsoon (ISM) is the heavy rainfalls that dominate the weather of Bangladesh and northeast India between late May and September. The trend towards a higher proportion of extreme rainfall events, with associated hazards and crop destruction, means that understanding monsoon dynamics on a range of timescales is of critical importance both for the production of useful future monsoon predictions [*Goswami et al*., 2006a] and to our understanding of the mechanisms that control monsoon variability. On longer timescales (greater than a thousand years), the majority of our knowledge of the controls on monsoon intensity come from proxy records that do not directly relate to precipitation volume. Rather, these record productivity/upwelling [e.g., *Clemens and Prell*, 2003; *Ziegler et al*., 2010], which may relate to surface wind stress or nutrient delivery [see *Caley et al*., 2011a], or—in the case of speleothems [*Wang et al*., 2008, 2001]—precipitation amount, source, and terrestrial water recycling of both the winter and summer Asian monsoons [*Pausata et al*., 2011; *Clemens et al*., 2010]. The oxygen isotopic composition ($\delta^{18}O$) of foraminifera from the Bay of Bengal, e.g., *Kudrass et al*. [2001], is difficult to interpret because shifts may be due to changes in either the amount of precipitation or the $\delta^{18}O$ of the freshwater source. Notwithstanding the wealth of information regarding monsoon intensity variation over the past 500 ka from such studies, an independent record of freshwater flux is required.

The ISM is driven by sensible heating of the Asian landmass, resulting in a tropospheric pressure gradient between Asia and the equator, and strong southwesterlies that carry moisture from the equatorial Indian Ocean and Arabian Sea. As these air masses rise over the Himalayas, the condensation of water vapor transported from these oceans transfers latent heat to the atmosphere, further driving the low-pressure system over Asia [*Webster*, 1994]. Extended India monsoon rainfall, defined as all rain falling within 70–100°E, 10–30°N

between June and August [*Goswami et al.*, 1999], is strongly correlated with the area under the curve defined by the difference in tropospheric temperature (integrated over 200–600 hPa) between 10–35°N and 14°S–10°N at 30–100°E, whilst this difference is positive [*Goswami et al.*, 1999]. This is itself closely related to the extent to which the North Atlantic Oscillation (NAO) controls the summer low pressure over Eurasia. A model constructed around these variables provides a mechanism for interannual variability in monsoon precipitation at present, which is principally driven by the magnitude and extent to which the positive tropospheric temperature anomaly persists through August–October. On orbital timescales, monsoon proxy records are forced in part by low-latitude northern hemisphere summer insolation [e.g., *Wang et al.*, 2008]. However, different proxies lag insolation maxima by differing amounts, particularly within the precession band [e.g., *Bolton et al.*, 2013]. In order to address current uncertainties regarding the potentially indirect relationship between existing palaeomonsoon indices and precipitation amount/source (as opposed to wind stress), we have produced the first direct reconstructions of central Bay of Bengal Ba/Ca_{sw} (proportionally related to salinity), based on planktic foraminifera Ba/Ca measurements. Using these data to validate the relationship between salinity and previously published $\delta^{18}O$ data sets through MIS3 enables us to examine the orbital controls on ISM precipitation amount over the last 80 ka for the first time.

Planktic foraminifera Ba/Ca (Ba/Ca_{test}) is a promising proxy for salinity because test Ba/Ca appears to be dependent only on seawater Ba/Ca (Ba/Ca_{sw}) [*Hönisch et al.*, 2011], i.e., temperature, pH, and other variables exert no resolvable control on Ba/Ca_{test}. Previous attempts have been successful in reconstructing changes in freshwater flux to the surface ocean through time by analysing the Ba/Ca ratio of surface-dwelling foraminifera [*Weldeab et al.*, 2007; *Hall and Chan*, 2004]. This is because (1) bulk seawater Ba/Ca can be assumed to have remained constant over glacial-interglacial timescales because of the residence times of these elements [*Li*, 1982], and (2) rivers are characterized by [Ba] greater than that of seawater [e.g., *Singh et al.*, 2013]. Therefore, foraminifera Ba/Ca may be used as an indicator of changes in freshwater flux through time.

The central Bay of Bengal represents a good location with which to track changes in ISM freshwater flux as it is sufficiently distal from the coast to be sensitive to freshwater flux irrespective of shifts in the focus of precipitation through time. We present a Ba/Ca-derived freshwater and Mg/Ca-derived temperature record from 68 to 45 ka, based on laser-ablation inductively coupled plasma mass spectrometry (LA-ICPMS) measurements of the surface-dwelling foraminifera *Globigerinoides ruber*. This represents the most recent period of time that was characterized by a more intense Indian monsoon than the Holocene [*Caley et al.*, 2011a]. We utilize core RC12–343 (15.17°N, 90.57°E, 2666 m depth) for which foraminifera $\delta^{18}O$ and ϵNd data are already available [*Stoll et al.*, 2007a]. We compare our data to freshwater flux calculations based on $\Delta\delta^{18}O$ (residual $\delta^{18}O$; the difference in $\delta^{18}O_{test}$ between a given core site and a location with a similar temperature evolution but no freshwater influence), derived from previously published data sets. This enables us to build a more complete picture of freshwater input to the Bay of Bengal through time, with sufficient data to examine the control that orbital forcing exerts on quantitative reconstructions of monsoon precipitation, averaged over several large drainage basins.

2. Materials and Methods

At present, the core location is characterized by a 28.2°C mean annual sea surface temperature (SST). Salinity and $\delta^{18}O_{sw}$ are modified by freshwater input to the Bay of Bengal, principally from the Ganges-Brahmaputra system. The average annual salinity is 32.3‰ [*Locarnini et al.*, 2013]. *G. ruber* are known to be resilient to low-salinity seawater and do not change their habitat of depth in response to salinity variation [*Schmuker and Schiebel*, 2002]. We focus on *G. ruber* for SST and freshwater reconstruction throughout the analyzed core intervals, whilst also producing LA analyses and SEM images for *Globigerinella siphonifera* in order to assess foraminifera preservation in detail at this site.

Foraminifera were analyzed from eight intervals of core RC12–343 between 68.0 and 43.9 ka. These intervals represent a subset of the same samples from which foraminifera were selected for the ϵNd and $\delta^{18}O$ data of *Stoll et al.* [2007a] and are therefore equivalent in terms of age.

2.1. Core Site Sedimentation Style

The core site is characterized by bulk sediment $CaCO_3$ of 30% at present and 10–20% over the sampled interval. The central Bay of Bengal is characterized by unusually high fluxes of organic carbon relative to

$CaCO_3$ to deep sediment traps [*Unger et al*., 2003; *Klaas and Archer*, 2002], because unlike most open ocean systems in which carbonate ballasting dominates [*Francois et al*., 2002], in the Bay of Bengal ballasting is likely enhanced by lithogenic material from the Ganges-Brahmaputra system [*Ittekkot et al*., 1991]. This environment results in a highly variable abundance of foraminifera. Following previous work [*Stoll et al*., 2007b], sufficient foraminifera were not present in several intervals over the last 80 ka, which means that a higher resolution trace element record from this core is not possible. Post-Last Glacial Maximum samples were not sufficiently abundant to sample with the exception of one interval at 12.8 ka.

In addition, as a result of this higher ratio of $C_{org}/CaCO_3$, the early diagenetic environment for carbonates of the Bay of Bengal differs from that typical of open ocean environments. Furthermore, the remineralization of the C_{org} between 150–1000 m and at depth is a contributing factor to the very low-oxygen concentration in the Oxygen Minimum Zone (OMZ) [*Sarma*, 2002] and may have implications for foraminifera preservation. This respiration is likely to promote carbonate dissolution and means that in sites such as these a microanalytical approach to trace element work is desirable in order to interpret data with confidence. This is especially the case as orbital-scale variability in monsoon intensity and wind strength are likely to result in preservational variability at or below the sampling resolution. Such issues may be common to all regions where foraminifera Ba/Ca data are useful for elucidating freshwater flux, as significant freshwater input is likely to be associated with high sedimentation rates and C_{org} burial; careful assessment of preservation is critical and high-resolution records may be difficult to produce.

2.2. Analytical Methodology

Prior to laser-ablation analysis, several cleaning protocols were tested in order to assess their effectiveness at removing clay/silicate particles and Fe-Mn-rich coatings. Aggressive oxidative/reductive procedures were avoided because laser-ablation analyses are sufficiently spatially resolved to enable the identification and exclusion of poorly preserved portions of individual chambers, and it has been shown that more aggressive cleaning procedures offer little or no benefit in terms of data quality compared to simply ultrasonicating specimens in methanol when using this analytical technique [*Vetter et al*., 2013]. We selected 65 *G. ruber* specimens from the 49.8 ka interval and split them into five groups to which different treatments were applied. Specifically, group (1) 4 $\times$ 1 min ultrasonication in H_2O, (2) 4 $\times$ 2 min ultrasonication in H_2O, (3) as group one with an extra 1 $\times$ 1 min ultrasonication in methanol and a 1 $\times$ 1 min ultrasonication rinse in H_2O, (4) as group three but with an extra 1 $\times$ 1 min ultrasonication in acetone between the final methanol and H_2O steps, and (5) no cleaning procedure applied. Samples were rinsed with H_2O in between the 1–2 min ultrasonications. At all stages only 18.2 MΩ deionized water was used for rinsing and ultrasonication. All cleaning procedures were found to have a large effect on measured X/Ca ratios compared to foraminifera to which no pretreatment was applied, see the supporting information for further details. Reliable trace element data can clearly not be obtained from uncleaned foraminifera. Briefly, B-Mg-Al-Zn-Ba/Ca were lower in all of the groups which had some cleaning applied whilst there was no significant shift in Li-Sr-Ce/Ca. There was little dependence of measured X/Ca ratios on the specific cleaning procedure applied, with the exception of Al/Ca which was far lower following the second cleaning procedure outlined above (treatments 1–5 have mean Al/Ca of 0.39, 0.014, 0.13, 0.079, and 0.32 mmol mol^{-1}, respectively). The effectiveness of technique 2 (4 $\times$ 2 min ultrasonication in deionized water) at removing clay particles, which are the likely source of Al/Ca contamination, is probably due to the longer ultrasonication steps in deionized water. The high viscosity of water compared to acetone or methanol is presumably the reason that this simple technique was found to be the most effective at removing contaminant phases. Consequently, this technique was chosen to clean the specimens used for trace element measurements through the core.

Cleaned foraminifera were mounted onto a glass slide using double-sided carbon tape and air-dried before laser-ablation. The LA-ICPMS setup at RHUL features a RESOlution M-50 prototype laser-ablation system connected to an Agilent 7500 ICPMS, and has been previously described in detail [*Müller et al*., 2009]. Laser-ablation and ICPMS parameters did not differ from those previously reported, with the exception of the additional diatomic gas which was changed from N_2 to H_2 in order to reduce the m/z = 55 background to obtain the best possible ^{55}Mn data [*Evans and Müller*, 2013]. Laser-ablation depth profiling through the test was carried out using a 57 μm laser spot size and a repetition rate of 2 Hz in order to maximize spatial resolution; fluence was ~3.5 J cm^{-2}. In total, 164 specimens were analyzed (~20/sampled interval). Standardization was performed using NIST610 and NIST612, the MPI-DING komatiite glass GOR132 [*Jochum et al*., 2006] was used to assess accuracy, see the supporting information for details. Laser-ablation depth profiling

accuracy and precision relating specifically to analytical protocols used for foraminifera analysis are described in detail in *Evans et al*. [2015], including a discussion of the effect of updated NIST concentration values on data quality [*Jochum et al*., 2011].

Temperature was derived from Mg/Ca analyses using the calibrations of *Kisakürek et al*. [2008] for *G. ruber* and *Elderfield and Ganssen* [2000] for *G. siphonifera*. We do not utilize a Mg/Ca-temperature calibration that incorporates a dissolution correction as our spatially resolved laser-ablation data and SEM images enable us to avoid poorly preserved samples. Mg/Ca-derived temperature errors are ±2 SE of all measurements from a given core interval.

3. Results

3.1. Assessing Preservation: LA X/Ca Analyses and SEM Imaging

Laser-ablation analysis of foraminifera is becoming an increasingly popular analytical tool because of its power to assess both interchamber and intrachamber variation in commonly applied proxy X/Ca ratios, at a resolution of better than 1 μm when depth profiling [e.g., *Eggins et al*., 2003; *Reichart et al*., 2003; *Evans et al*., 2015]. Such studies commonly use modern core-top, plankton tow or sediment-trap foraminifera as a reference point for the quality of preservation in the fossil record. Consequently it is frequently assumed that the best data are those characterized by low Al-Fe/Ca and Mn/Ca ratios, which are typically used as indicators of silicate mineral contamination and secondary carbonate overgrowths [*Pena et al*., 2005; *Barker et al*., 2003; *Creech et al*., 2010; *Hollis et al*., 2009].

Figure 1 shows the relationship between textural preservation as observed in SEM images and Mg/Ca, Al/Ca, and Mn/Ca in chamber wall LA depth profiles. Several distinct styles of preservation can be recognized, which presumably relate to differential diagenetic processes. All specimens analyzed by LA-ICPMS show some degree of alteration, albeit sometimes only in the very low-concentration trace elements such as U, and the question is therefore: to what extent can complex differential diagenesis be identified in laser-ablation profiles?

Well-preserved specimens are characterized by proxy X/Ca ratios within the range of pristine nonfossil material but elevated Mn/Ca (Figure 1a; 0.06–0.5 mmol mol^{-1} cf. 0.02 mmol mol^{-1} in plankton tow *G. ruber* [*Eggins et al*., 2003]). Dissolution of some specimens is evident in SEM images, however overall there is no discernible effect on any of the proxy trace elements (Figure 1b). Whilst it has been shown that dissolution can lower Mg/Ca ratios below a certain bottom water $\Delta[CO_3^{2-}]$ threshold [*Regenberg et al*., 2014], we observe specimens both with and without evidence of dissolution throughout the sampled intervals. Consequently, we do not apply a correction here as some specimens are unambiguously unaffected (Figure 1a) and there is no evidence based on our profiles that some elements are leached preferentially to Ca, although this has been demonstrated at other locations [*Fehrenbacher and Martin*, 2014]. Subtle submicrometer reorganization of the chamber walls to a more granular texture, which is difficult to discern under optical microscopy, is associated with substantial (>50%) Mg loss and Y-REE, Ba, and U enrichment. Mn/Ca may be elevated above that of the visually well-preserved material whilst Al/Ca is broadly unaffected.

These comparative laser-ablation analyses and SEM images highlight the need for careful use of Al/Ca and Mn/Ca as alteration indicators. Whilst specimens that have undergone recrystalization are characterized by elevated Mn/Ca ratios in some cases, those with the lowest Al-Mn/Ca are often individuals exhibiting dissolution. Although not a problem at the site utilized here, this has the potential to bias results in sample sets where dissolution substantially biases proxy trace elements. Furthermore, core-top specimens are characterized by unrealistically low temperatures (mean *G. ruber* Mg/Ca = 2.0 ± 0.34 mmol mol^{-1}, equivalent to ~16°C), and yet these have mean Mn/Ca = 0.015 mmol mol^{-1}, the lowest of any sampled interval. We do not observe such poorly preserved foraminifera in any other interval, although this does serve to highlight that low Mn/Ca ratios do not always indicate good preservation. Ideally, laser-ablation data should be associated with wall microstructure SEM images in order to match trace element signatures with diagenetic style. Low Al-Mn/Ca may be an indication of good preservation [*Pena et al*., 2005], however we demonstrate that this conclusion cannot be drawn independently of careful coupling of geochemical analysis with SEM imagery.

Using all of these observations, a quantitative method of data exclusion was developed in order to avoid bias from analyses affected by any manifestation of diagenesis. A key feature of this method is that it is

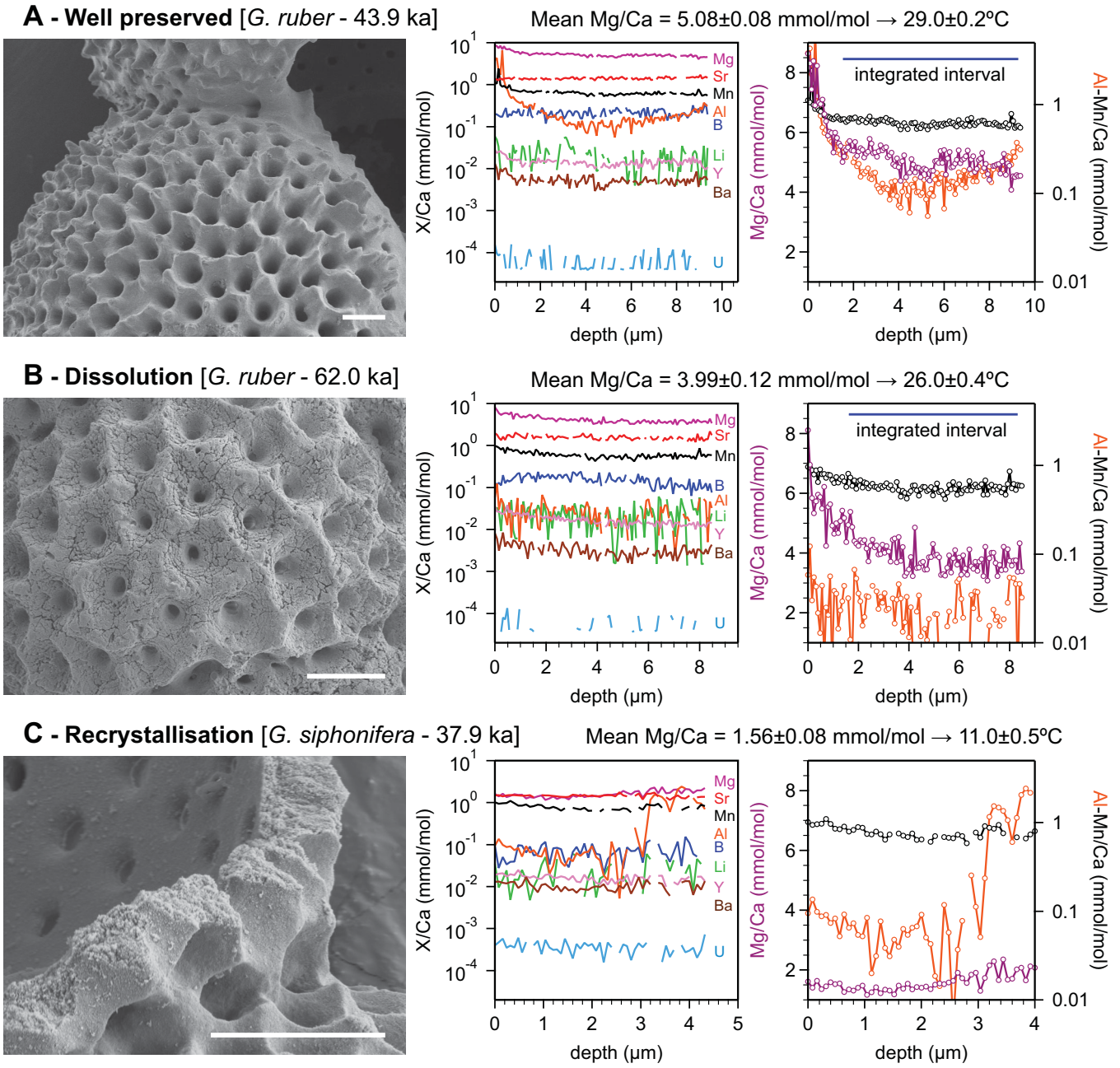

Figure 1. Comparative textural (SEM images) and chemical (laser-ablation depth profiles) characteristics of planktic foraminifera from core RC12–343. All preservation states were typically found in each sampled interval. These comparisons highlight the requirement of LA data in the context of wall microtexture, and vice versa. Note that some poorly preserved foraminifera, namely those that have undergone micrometer-scale recrystallization (c), appear superficially well-preserved if broken chamber walls are not examined. Minor dissolution was not found to significantly impact proxy trace element data present at concentrations >50 μmol mol^{-1}. SEM images are of the same specimens from which LA data are derived, although different chambers have been selected for clarity. Scale bars are 10 μm.

noncircular, i.e., Mg/Ca analyses that gave unreasonably low temperatures were not excluded *a priori*. This process was performed in two stages. First, each LA depth profile was assessed in order to identify areas of correlation between Mg/Ca and any of Al-Mn-Y-REE/Ca. These intervals were excluded as such correlation implies intrachamber trace element alteration. Second, the mean of all remaining data from each individual laser-ablation depth profile was used to exclude: (1) analyses with Al/Ca >0.3 mmol mol^{-1} which are those with remnant silicates, (2) analyses with Y/Ca >30 μmol mol^{-1} which have significant Mn-Y-REE-rich overgrowths, (3) analyses with Mg/Ca RSD >40% which were typically very short and noisy analyses during which the chamber shattered during ablation, and (4) analyses with Mn/Ca <30 μmol mol^{-1} (such as the

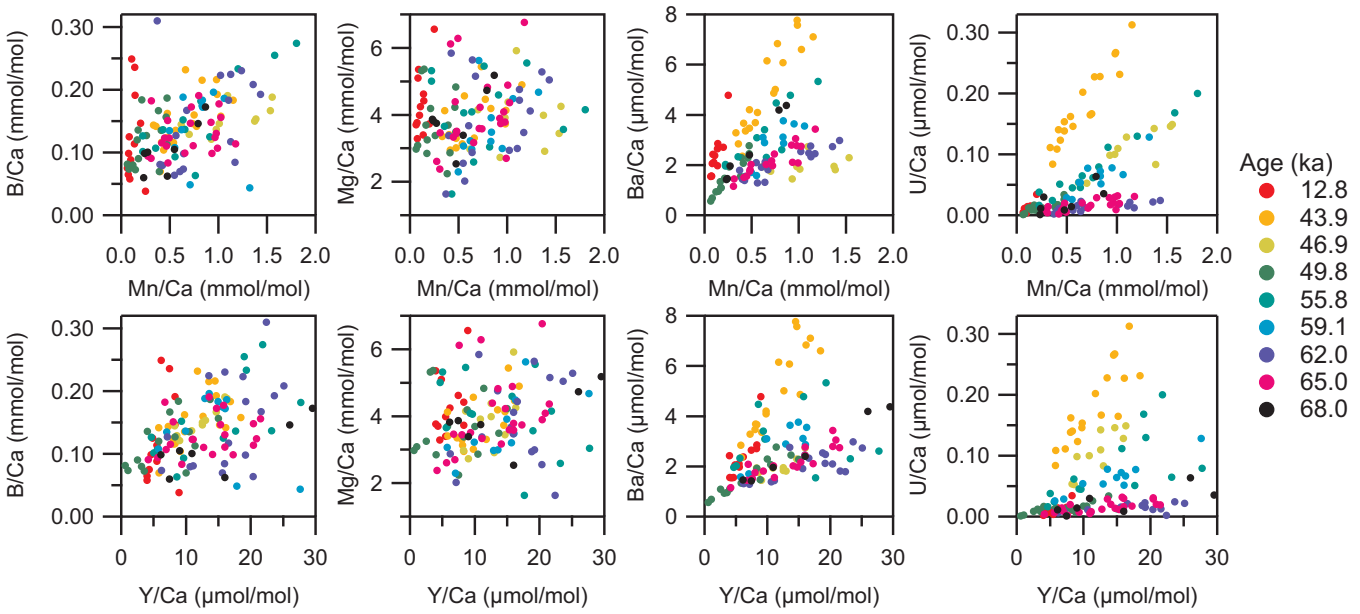

Figure 2. The relationship between B, Mg, Ba, U, and two trace elements commonly used as diagenesis indicators (Mn and Y) for all sampled intervals between 12.8 and 68 ka. B/Ca and Mg/Ca show no correlation with either Mn/Ca or Y/Ca (with the exception of B/Ca at 46.9 ka), implying no consistent diagenetic control on these ratios. Ba/Ca and U/Ca show strong interval-specific correlations with both Mn/Ca and Y/Ca. Trace element ratios present at primary concentrations of less than ~10 μmol mol^{-1} are largely controlled by diagenesis.

core top specimens) as these may have undergone substantial recrystallization. Using this methodology, 24% of all analyses were discarded and the mean Mg/Ca value for any given sampled interval was shifted by up to ~0.4 mmol mol^{-1} (~1°C) compared to the mean of all analyses. Although intrashell heterogeneity in *G. ruber* Mg/Ca has been reported [*Eggins et al*., 2003; *Fehrenbacher and Martin*, 2014], this is generally less than 2 RSD of 80% and therefore exclusion criteria (3) does not remove useful analyses. Similarly, whilst *Fehrenbacher and Martin* [2014] report a Mg/Ca RSD of up to ~60% for Holocene specimens, these microprobe-derived maps have a higher lateral spatial resolution than laser-ablation depth profiles. Our unpublished analyses of plankton tow *G. ruber* have Mg/Ca 2 RSD of 11–36%, similar to well-preserved specimens from core RC12–343 which are characterizsed by Mg/Ca 2 RSD of 23.0 ± 14.7%.

Based on correlations with Mn/Ca and Y/Ca, low concentration (<10 μmol mol^{-1}) X/Ca data may be unreliable (Figure 2), although see discussion of Ba below for exceptions to this. Conversely, there is no indication that Li, B, Mg, or Sr have been altered. Whilst it is evident from our data that no specimens are perfectly preserved, we demonstrate that it is possible to obtain useful proxy data from variably preserved material when using microanalytical techniques [see also *Kozdon et al*., 2011].

3.2. Primary Test Ba/Ca Reconstruction

Using planktic foraminifera test chemistry as an indication of palaeomonsoon intensity requires the freshwater flux to the Bay of Bengal to be constrained. The present-day salinity-δ^{18}O relationship provides an indication of freshwater flux through time, however it is not known to what extent uncertainties regarding temporal change in the isotopic composition of the freshwater in the past may bias these data. Therefore, an independent proxy for freshwater flux is required. We utilize Ba/Ca for the reasons outlined above.

This technique is complicated in this case because the low-concentration (sub-100 μmol mol^{-1} X/Ca) trace element ratios are elevated and correlate well with X/Ca ratios typically used as diagenetic indicators (Figure 2). However, because Ba/Ca is tightly linearly correlated with Y-REE/Ca (mean R^2 of all sampled intervals = 0.82 for Ba/Ca-Nd/Ca), these trends can be used to reconstruct the primary Ba/Ca ratio of these samples. Y-Ba/Ca and Nd-Ba/Ca covariance for all intervals which contain enough data points for this relationship to be tightly constrained is shown in Figure 3.

Whilst there is demonstrably more than one style of preservation, there are no inflection points in the Ba-Mn-Y-REE/Ca plots (Figures 2 and 3), therefore a linear regression is suitable for primary Ba/Ca reconstruction. Doing so requires knowledge or assumption of the primary Y/Ca and Nd/Ca ratios in order to define

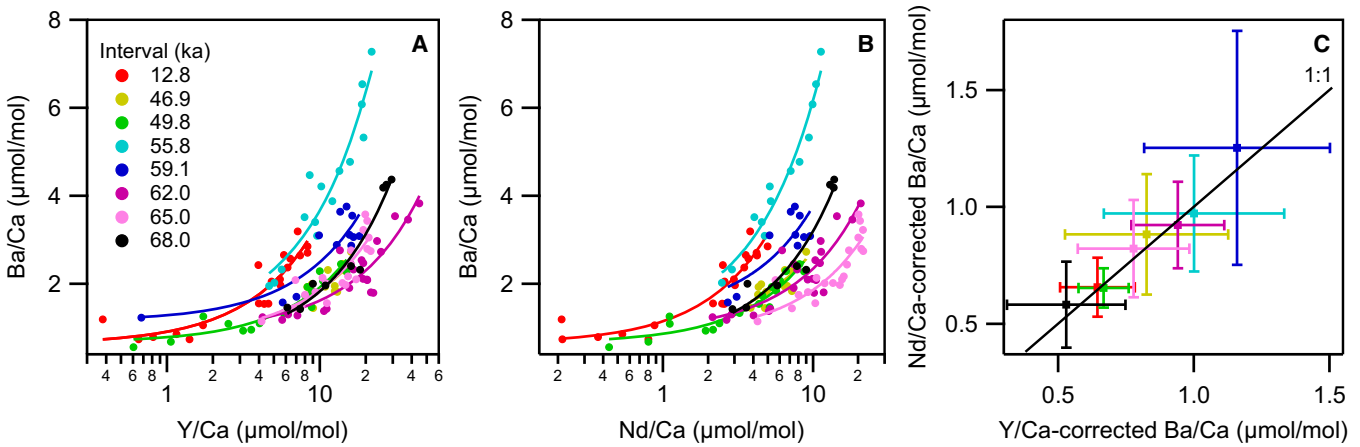

Figure 3. Reconstructing primary test Ba/Ca in diagenetically altered foraminifera using the linear relationship between (a) Ba/Ca-Y/Ca and (b) Ba/Ca-Nd/Ca. See text for the assumptions regarding primary Y/Ca and Nd/Ca ratios used to derive the primary Ba/Ca reconstructions in (c).

the intersection point of the Ba-Y-Nd/Ca regressions. We use the Nd/Ca value of *Pomiès et al.* [2002] (8 nmol mol^{-1}) and in the absence, to our knowledge, of any published Y/Ca data for live-collected foraminifera, a primary Y/Ca value derived from the lowest foraminiferal La/Ca value of *Palmer* [1985] (50 nmol mol^{-1}). Despite uncertainty regarding these primary ratios, our reconstructions are insensitive to the chosen value, and therefore to potential changes in primary foraminiferal Y/Ca and Nd/Ca in the past. For example, assuming a primary Nd/Ca value of 16 instead of 8 nmol mol^{-1} shifts our Ba/Ca values by ~0.01 μmol mol^{-1}, an error which is an order of magnitude smaller than that derived from the uncertainty in the regressions. The errors in our primary Ba/Ca_{test} values are defined by taking into account the uncertainty in both the slope and the intercept of each individual regression. Correcting the Ba/Ca data using either Y/Ca or Nd/Ca produces almost identical reconstructions (Figure 3c and Table 1) indicating that the technique is robust. We therefore demonstrate the power of laser-ablation not only as a microanalytical tool capable of identifying intratest diagenetic variability, but also as a technique that facilitates the reconstruction of low-concentration primary foraminiferal X/Ca ratios through the accurate characterization of diagenetic phases. Although it is preferable to analyze pristine samples, it is becoming clear that these may not be as ubiquitous as previously thought [*Pearson et al.*, 2001; *Kozdon et al.*, 2011]. As an alternative, we show that subtly altered material can yield useful low-concentration trace element data. Table 1 shows regression parameters and uncertainties used to define primary Ba/Ca_{test} for all intervals, along with associated mean Mg/Ca measurements.

Finally, Ba/Ca_{sw} was calculated from corrected Ba/Ca_{test} using $D_{Ba} = 0.15$ [*Hönisch et al.*, 2011; *Lea and Spero*, 1994]. This distribution coefficient is derived from three species of planktic foraminifera which show

Table 1. Mg/Ca-Temperature Data (Using the Calibration of *Kisakürek et al.* [2008]) and Ba-Y and Ba-Nd Regression Parameters Used to Calculate Primary Test and Seawater Ba/Ca, See Text for Details.[a]

Age		Mg/Ca	Temp.	Ba-Y			Ba-Nd			Ba/Ca_{sw}		$\Delta\delta^{18}O$
(ka)	n	(mmol mol^{-1})	(°C)	m	$c\times10^{-4}$	R^2	m	$c\times10^{-4}$	R^2	Ba-Y	Ba-Nd	F_f
12.8	12	4.27 ± 0.47	26.8	0.28 ± 0.03	6.3 ± 1.4	0.861	0.50 ± 0.04	6.5 ± 1.3	0.877	4.4	4.5	−0.27
43.9	18	3.77 ± 0.34	25.3	0.36 ± 0.05	7.5 ± 6.0	0.752	0.70 ± 0.10	1.1 ± 0.5	0.738			7.3
46.9	10	3.89 ± 0.58	25.6	0.10 ± 0.03	8.2 ± 3.0	0.595	0.19 ± 0.04	8.8 ± 0.2	0.646	5.6	6.0	16.6
49.8	15	3.67 ± 0.47	24.9	0.13 ± 0.01	6.6 ± 0.9	0.886	0.21 ± 0.02	6.5 ± 0.8	0.906	4.5	4.5	11.1
55.8	13	3.96 ± 0.62	25.9	0.27 ± 0.03	9.9 ± 3.3	0.899	0.52 ± 0.03	9.7 ± 2.5	0.954	6.8	6.6	12.9
59.1	11	3.63 ± 0.56	24.8	0.13 ± 0.04	11.7 ± 5.1	0.614	0.25 ± 0.07	12.5 ± 5.0	0.732	7.9	8.5	19.0
62.0	17	3.81 ± 0.60	25.4	0.07 ± 0.01	9.4 ± 1.7	0.781	0.14 ± 0.02	9.2 ± 1.9	0.756	6.4	6.3	7.0
65.0	22	4.25 ± 0.52	26.8	0.10 ± 0.01	8.2 ± 2.1	0.767	0.11 ± 0.01	7.7 ± 2.1	0.764	5.3	5.6	10.5
68.0	7	3.67 ± 0.59	24.9	0.31 ± 0.03	2.6 ± 2.8	0.948	0.14 ± 0.01	3.7 ± 1.8	0.935	3.6	4.0	7.3

[a]The unit for the intercept of these regressions is μmol mol^{-1}. The number of analyses represents the number of (partially) well-preserved chambers, not the total amount analyzed. Ba/Ca_{sw} reconstructions are derived from these regressions using the Ba distribution coefficient of *Hönisch et al.* [2011]. No reconstruction is given for 43.9 ka as the Y-Nd/Ca-Ba/Ca regression cover a small range of Y-Nd/Ca ratios for this interval. F_f denotes freshwater volume percentage at the core site derived from $\Delta\delta^{18}O$ following *Stoll et al.* [2007a], assuming constant end-member composition through time.

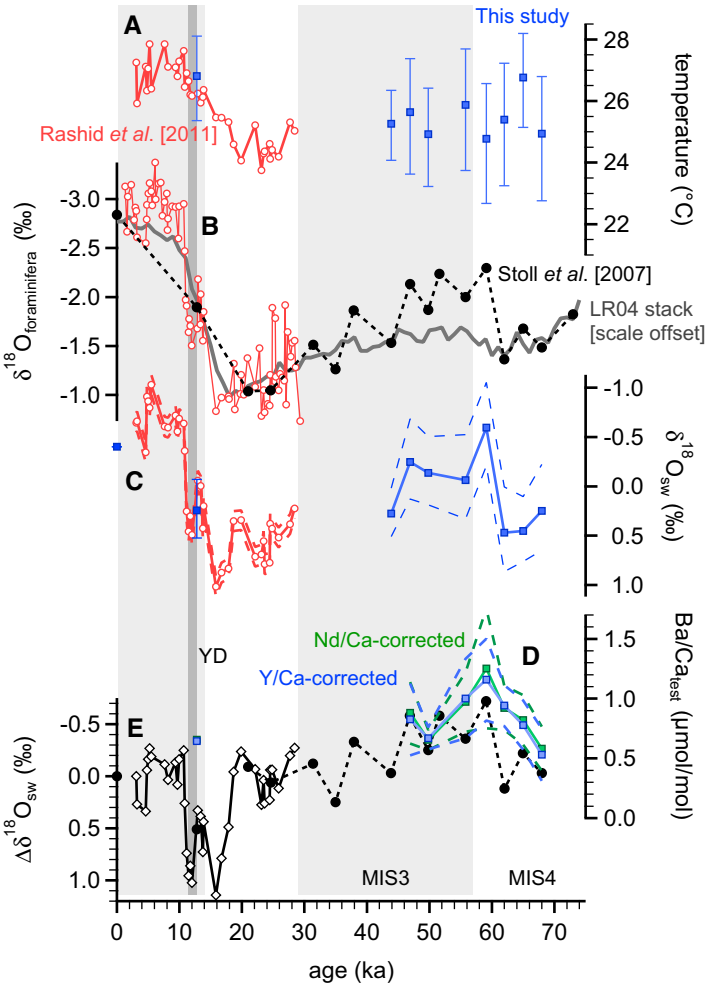

Figure 4. Foraminifera-derived reconstructions for the central/western Bay of Bengal. (a) Mg/Ca-derived temperature (this study and *Rashid et al.* [2011]). (b) $\delta^{18}O$, with the LR04 stack shown for comparison [*Lisiecki and Raymo*, 2005]. (c) $\delta^{18}O_{sw}$ calculated using data from *Rashid et al.* [2011] and *Stoll et al.* [2007a]. (d) Ba/Ca reconstructions (this study) and (E) $\Delta\delta^{18}O_{sw}$, which shows the difference between these $\delta^{18}O_{sw}$ records and that of ODP Site 758, an equatorial Indian Ocean site which is assumed to have an equivalent thermal evolution whilst devoid of freshwater influence [*Chen and Farrell*, 1991]. A negative $\Delta\delta^{18}O_{sw}$ value indicates a relatively more intense monsoon if the oxygen isotopic composition of the freshwater discharged into the Bay of Bengal is invariant through time (see text for details).

no significant offset from each other. The potential influence of temperature, salinity, pH, and $[CO_3^{2-}]$ on Ba/Ca_{test} exert an effect smaller than analytical uncertainty [see *Hönisch et al.*, 2011].

3.3. Mg/Ca-Temperature and $\delta^{18}O_{sw}$ Reconstruction

Mg/Ca-derived palaeotemperature estimates for the sampled intervals of RC12–343 are shown in the context of previously published Mg/Ca data from the Bay of Bengal [*Rashid et al.*, 2011] in Figure 4, along with available $\delta^{18}O$ records for the central/western part of the bay [*Stoll et al.*, 2007a; *Rashid et al.*, 2011]. Seawater $\delta^{18}O$ was calculated using the $\delta^{18}O_{c-sw}$-temperature calibration of *Erez and Luz* [1983]. The residual oxygen isotope record ($\Delta\delta^{18}O$) is derived in a similar manner to that previously described [*Stoll et al.*, 2007a; *Colin et al.*, 1999]. Briefly, the ice volume component is subtracted from Bay of Bengal $\delta^{18}O_c$ using foraminifera data from ODP Site 758 [*Chen and Farrell*, 1991], assuming equivalent temperature evolution of the Bay of Bengal and the equatorial Indian Ocean [see *Barrows and Juggins*, 2005; *Saraswat et al.*, 2005]. All data were normalized to present-day $\delta^{18}O_{sw}$.

Our MIS4/3 SST reconstructions range between 24.8 and 26.8°C and indicate that surface ocean temperatures at the core location were stable within error over the period 68–44 ka, despite large variations in $\delta^{18}O_{sw}$ over the same interval ($\sim 1‰$). These data are consistent with the magnitude of glacial cooling observed in other areas in the Bay of Bengal [*Rashid et al.*, 2011]. Together these records imply that surface ocean warming in the Bay of Bengal of 2–3°C occurred over the past ~15 ka, preceded by a period of relatively stable SST between ~25 and 26°C since at least ~65 ka. There is no evidence based on our data of temperature shifts of the magnitude observed over the last deglaciation during MIS4-3.

The Bay of Bengal $\Delta\delta^{18}O$ record (Figure 4) is offset to $\sim -0.5‰$ for the period 60–45 ka and is accompanied by a large negative shift in $\delta^{18}O_{sw}$ at 60–55 ka. In isolation this record may be equally explained by one or a combination of (1) increased monsoon intensity (i.e., a greater flux of freshwater to the Bay of Bengal), (2) a shift in the mean $\delta^{18}O$ of monsoon precipitation toward more negative values resulting from any combination of changes in: source $\delta^{18}O_{sw}$, precipitation altitude, atmospheric temperature, or the amount or extent of continental freshwater recycling, or (3) a negative shift in the oxygen isotopic composition of the Ganges-Brahmaputra river water resulting from a sustained pulse of isotopically light meltwater. As an

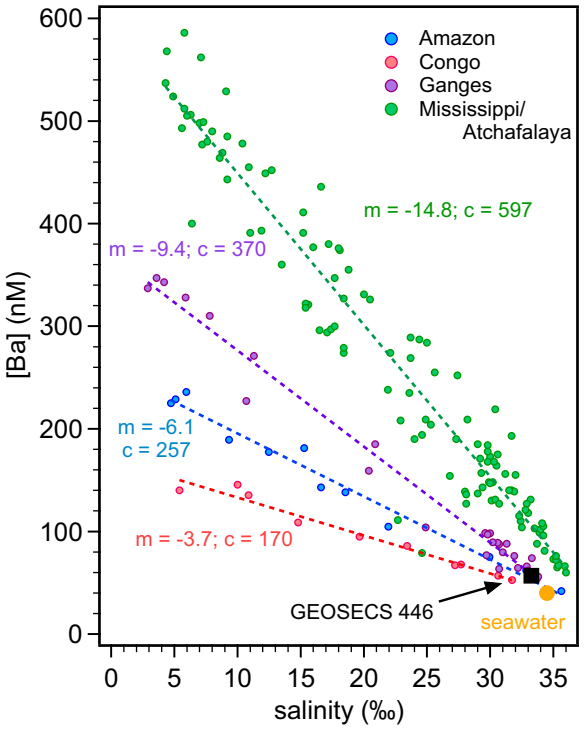

Figure 5. [Ba]-salinity relationships for four major (sub)tropical rivers [*Carroll et al*., 1993; *Hanor and Chan*, 1977; *Joung and Shiller*, 2014] and [*Edmond et al*., 1978, and references therein]. All rivers are characterized by low-salinity end-members with different [Ba], it is therefore essential that the end-member of the low-salinity source of interest is characterized before foraminifera-derived seawater Ba/Ca may be used to reconstruct salinity. GEOSECS station 446 (SW Bay of Bengal) falls on the Ganges-Brahmaputra low-salinity end-member-seawater mixing line, implying that short-period fluctuations in the slope of this relationship are not a complication for distal sites.

independent indicator of freshwater flux to the surface ocean, our foraminifera Ba/Ca record provides further constraint on this. These data show an increase in Ba/Ca_{test} from 0.52 to 0.82 μmol mol^{-1} for the period 68–65 ka to 0.97–1.25 for the period 59–56 ka and support the hypothesis that there was an increase in freshwater discharge into the Bay of Bengal around the onset of MIS3. Following this interval Ba/Ca_{test} returns to lower values of 0.65–0.88 μmol mol^{-1}.

4. Discussion

4.1. Freshwater Flux Reconstruction From Foraminifera Geochemistry

4.1.1. Foraminifera Ba/Ca Relationship to Freshwater Flux in the Bay of Bengal

Calculating the freshwater component from foraminifera Ba/Ca measurements requires knowledge of the freshwater end-member [Ba], which may be equivalent to constraining the Ba/Ca-salinity relationship if no other processes modify [Ba] in estuarine or deltaic mixing zones on kilo-year timescales. In the Bay of Bengal, Ba-salinity regressions indicate that a simplistic model for Ba flux to the surface ocean may not accurately represent the processes that result in elevated Ba/Ca_{sw}. Whilst *Carroll et al*. [1993] and *Moore* [1997] report river (i.e., salinity = 0‰) [Ba] between 110 and 167 nM, the Ba-salinity regression indicates a low-salinity component with much higher [Ba]. This is shown in the context of other major (sub)tropical rivers in Figure 5. The high [Ba] of the low-salinity end-member in the Bay of Bengal relative to the Ganges-Brahmaputra is a consequence of Ba desorption from sediment [*Carroll et al*., 1993] and the incursion of saline, Ba-rich groundwater release during periods of low river discharge (December–May) [*Moore*, 1997]. Similarly, elevated [Ba] with respect to the freshwater source is evident in at least three other river systems [*Edmond et al*., 1978; *Hanor and Chan*, 1977], and *Joung and Shiller* [2014] highlight the complexity in seasonal Ba-salinity relationships for the Louisiana Shelf, a "worst-case scenario". However, whilst the slope of a [Ba]-salinity relationship undergoes short-period (sub)annual variations [*Moore*, 1997; *Joung and Shiller*, 2014], this may not be a complication on longer timescales, especially for more distal sites such as RC12–343, as (1) there is a finite degree of Ba desorption from sediment in both brackish mixing zones and subterrestrial groundwater reservoirs and (2) mixing is likely to average over these variations when the site is sufficiently far from the point source. This is visible in the data of *Joung and Shiller* [2014] which show much less scatter and seasonal variation within 5‰ of open ocean salinity. Furthermore, the Bay of Bengal is advantageous in this respect because the freshwater signal is large enough to be detected 100s of km away from the coast. Surface seawater [Ba] at GEOSECS station 446 (southwest Bay of Bengal; see *Saraswat et al*. [2013] and references therein), conforms exactly to the Ba-salinity relationship defined by the open-ocean waters of *Carroll et al*. [1993], see Figure 5. This implies short-period variations in the low-salinity end-member [Ba] do not translate into seasonally or annually variable open-ocean Ba-salinity fluctuations, especially because our data are derived from multiple individual foraminifera which are likely to have existed over several decades or centuries. Therefore, our data represent average freshwater fluxes on a timescale much greater than seasonal or interannual variation and can be considered to track long-term changes in seawater chemistry. This lack of (inter)annual variation at locations distal from the point source is because coastal groundwater aquifers are recharged

during periods of high freshwater flux, during which solution Ba adsorbs to sediment, whilst the opposite occurs when freshwater discharge is low and seawater infiltrates the aquifer [*Moore*, 2010]. Because desorption of Ba from sediment is fast [*Coffey et al*., 1997, and references therein], particularly in well-mixed shallow marine settings such as the northern Bay of Bengal, seawater [Ba] can still be expected to relate to freshwater flux when averaged over longer time-scales. Furthermore, seawater [Ba] is known to correlate well with freshwater flux over long timescales in systems for which data are available [*McCulloch et al*., 2003]. Whilst this may be a reasonable hypothesis, we do make the assumption that freshwater flux and Ba/Ca_{sw} covary linearly (i.e., a doubling in freshwater flux is associated with a doubling in river-derived Ba) when assessing variation in ISM intensity in the past based on our data, which is the case for other systems [*McCulloch et al*., 2003].

G. ruber is present in the Bay of Bengal year-round without significant seasonal bias in the flux of shells to the sea floor. For example, in the northern part of the bay, *Guptha et al*. [1997] found the flux of this species in the 250–500 μm size fraction (analyzed here) remained between $\sim$10 and 30 shells m^{-2} d^{-1} throughout the year. This is in contrast to *G. bulloides*, for example, which shows a strong seasonal bias in shell flux during June–August [*Guptha et al*., 1997]. Thus our *G. ruber* Ba/Ca data represent an estimate of mean annual freshwater flux averaged over several tens-hundreds of years for each analyzed interval.

Although the present-day Bay of Bengal low-salinity end-member [Ba] is well constrained, we do not use this to directly reconstruct salinity from our Ba/Ca data because there is evidence that freshwater flux to the Bay of Bengal was not dominantly sourced from the Ganges-Brahmaputra prior to the Holocene. Specifically, the ϵNd record from RC12–343 [*Stoll et al*., 2007a] shows a large glacial-interglacial difference, which has been interpreted as a result of a shift in the ITCZ in response to northern hemisphere warming. Such a shift may have resulted in a change in the dominant location of Indian monsoon precipitation from the Ganges-Brahmaputra to the Arakan and Irrawaddy drainage systems, which can explain the more radiogenic glacial ϵNd as well as the difference in $\Delta\delta^{18}O$ of the location of this core compared to that of a core in the Andaman Sea to the south-east [*Stoll et al*., 2007a; *Colin et al*., 1999]. These residual oxygen isotope records are broadly coherent on longer timescales but show an opposite trend toward the end of T1, which may also suggest a shift in the location of freshwater input at this time. Because of this shift in the focus of precipitation, an absolute comparison between our Ba/Ca_{sw} data and the $\Delta\delta^{18}O$ record, in freshwater flux terms is not possible.

Whilst this could be overcome if the [Ba] of all fluvial end-members is known, to our knowledge, there are no published [Ba] values for the Irrawaddy or Arakan systems that would enable us to test whether our Ba-derived freshwater record may be influenced by a shift in rainfall to the east, which may be characterized by rivers with [Ba] significantly different to the Ganges-Brahmaputra system (as different rivers are characterized by low-salinity end-members with highly variable [Ba]; Figure 5). This is also a potential complication for previous studies utilizing foraminifera Ba/Ca to reconstruct salinity proximal to river systems for which the low-salinity end-member was not known [*Weldeab et al*., 2007]. As an alternative, we use the slopes of the Ba-salinity relationships shown in Figure 5 to reconstruct a range of potential relative shifts in the freshwater component between 68 and 47 ka. We do not include the Mississippi Ba-salinity relationship in this calculation (Figure 5) because it does not trend back to seawater [Ba] at Indian Ocean salinity unaffected by riverine freshwater. Peak Ba/Ca_{sw} occurs at 59.1 ka (7.7–8.3 μmol mol^{-1}), which equates to a Ba/Ca_{sw} shift of $\sim$4.3 μmol mol^{-1} relative to 68 ka. A rise of this magnitude is equivalent to a 1.1–4.9‰ salinity drop. The core site is characterized by a present-day freshwater fraction of 0.064, assuming that ocean salinity in the absence of freshwater input in this region would be 34.5‰ as it is in the equatorial Indian Ocean. If the freshwater component at this location was similar to present day prior to this Ba/Ca_{sw} excursion, a salinity decrease of 1.1–4.9‰ implies that peak MIS3 freshwater flux to the core site was 1.5–3.2 times greater than modern.

4.1.2. Compositional Change in Fresh/Seawater Over T1 and MIS4/3

Our records of monsoon intensity are shown in the context of the NGRIP $\delta^{18}O_{ice}$ record [*Anderson et al*., 2004], the DSDP Site 609 detrital carbonate component [*Bond et al*., 1999], two ISM stacks [*Caley et al*., 2011a; *Clemens and Prell*, 2003] and the Wulu Cave $\delta^{18}O$ record [*Liu et al*., 2010] in Figure 6. Residual oxygen isotope records, as described above, were scaled to freshwater flux using the present-day mean oxygen isotopic composition of the Ganges-Brahmaputra, assuming negligible freshwater from other rivers at this site.

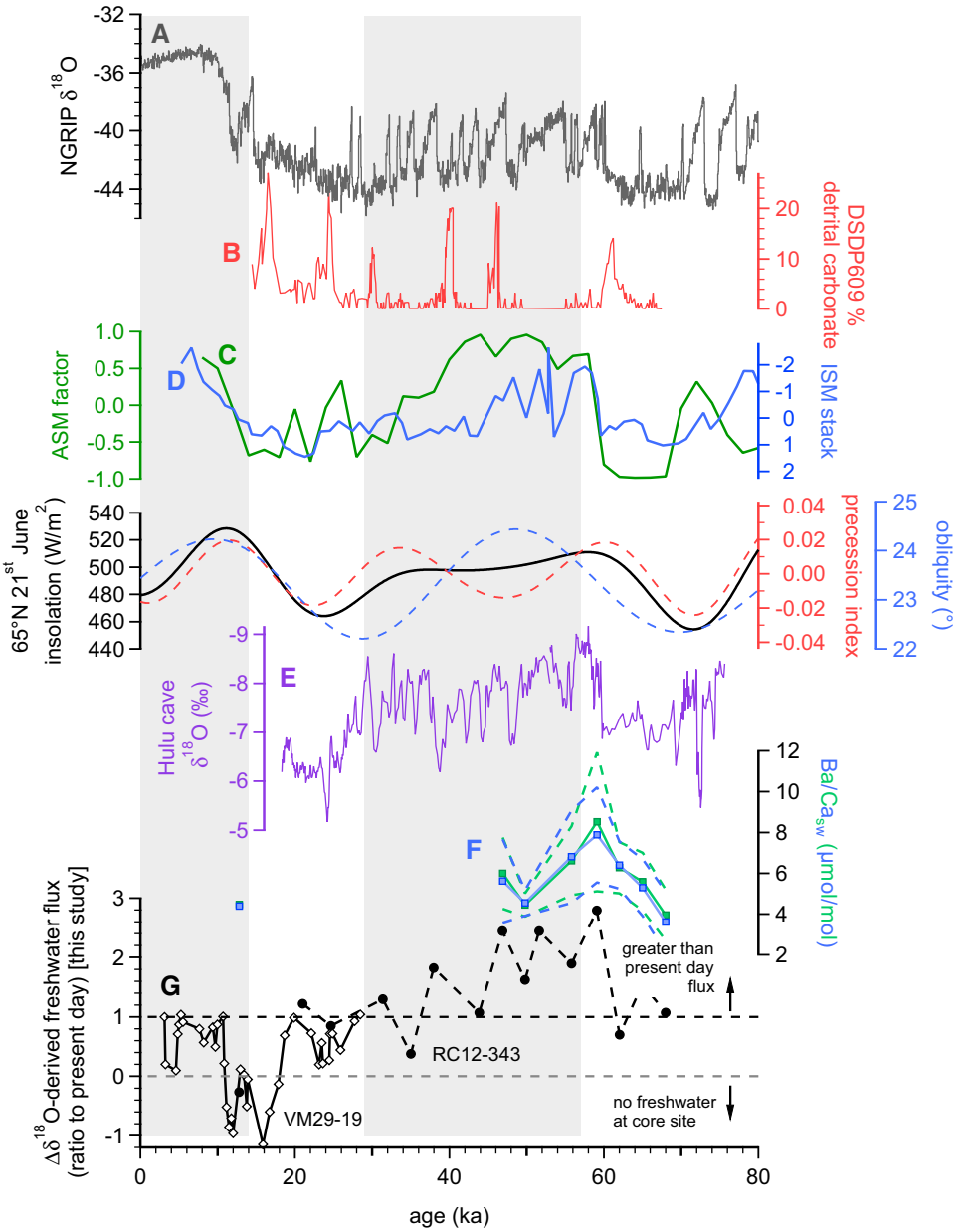

Figure 6. Bay of Bengal freshwater flux reconstruction in the context of previous climate/process proxies and Indian-Asian monsoon indices. (a) NGRIP δ^{18}O [*Andersen et al.*, 2004], (b) The DSDP Site 609 detrital carbonate grain component, an indicator of Heinrich events [*Bond et al.*, 1999], two multiproxy stacks of (c) Arabian Sea Summer Monsoon Factor [*Clemens and Prell*, 2003], and (d) Indian Summer Monsoon [*Caley et al.*, 2011a], (e) the Hulu Cave δ^{18}O record from southwest China [*Wang et al.*, 2001], and our reconstruction of changes in the freshwater component in the Bay of Bengal relative to present day derived from (f) foraminifera Ba/Ca and (g) $\Delta\delta^{18}$O (data from *Stoll et al.* [2007a] *Rashid et al.* [2011]).

This is defined by the intercept of the salinity-δ^{18}O relationship reported in *Delaygue et al.* [2001], which is $-5.9‰$.

Although we cannot use our Ba/Ca_{sw} record to independently test the absolute magnitude of the freshwater flux shown by the $\Delta\delta^{18}$O-derived freshwater flux calculations (Figures 6f and 6g), several features of these records means that it may be used to ascertain which aspect of the system the residual oxygen isotope data pertain to. Specifically, $\Delta\delta^{18}$O data are controlled by a combination of freshwater flux and changes in $\delta^{18}O_{freshwater}$ and may be associated with errors relating to a divergence in the secular SST evolution of the site to which these data are normalized (ODP Site 758). In this region, two main processes may affect $\delta^{18}O_{freshwater}$: a change in precipitation δ^{18}O or a change in the contribution from snowmelt to river

discharge. Recent modeling of changes in precipitation and $\delta^{18}O$ fractionation in response to sudden climatic events [*Pausata et al*., 2011] indicates that the oxygen isotopic composition of the freshwater end-member can be expected to change through time. Specifically, sudden cooling is predicted to result in less precipitation over the Indian Ocean and subcontinent, leading to a less fractionated precipitation over northern India and east Asia [*Pausata et al*., 2011]. This translates to a more positive riverine $\delta^{18}O$ and would lead to an underestimation of the freshwater flux during such periods if the shift in $\delta^{18}O_{freshwater}$ was large, given that there is evidence that this general difference in precipitation holds for prolonged colder periods [*Marzin et al*., 2013] and is not just a feature of Heinrich events.

In contrast, large-scale melting of Himalayan ice, with present-day $\delta^{18}O = \sim -18‰$ [*Thompson et al*., 2000] is unlikely to significantly affect freshwater $\delta^{18}O$ over long timescales; an increase from 1 to 5% current snowmelt contribution [*Siderius et al*., 2013] to 10% ice component of Ganges river discharge would be required to shift Ganges-Brahmaputra $\delta^{18}O$ by $\sim -1‰$, the equivalent to melting and draining all current Himalayan-Karakoram ice in a $<$60 year period based on the present-day ice volume estimates of *Frey et al*. [2014] and the current volume of Ganges discharge from *Siderius et al*. [2013].

Using these observations, we argue that $\Delta\delta^{18}O$ is more sensitive to freshwater flux than any other variable (e.g., changing source composition), and can therefore be used as a reliable indicator for the secular evolution of freshwater in the Bay of Bengal. This is the case for the following reasons:

1. The coherence of the timing of the Ba and $\Delta\delta^{18}O$-derived freshwater record strongly suggests that $\Delta\delta^{18}O$ records a shift in freshwater flux to the core site rather than, for example, a change in the oxygen isotopic composition of the freshwater end-member over this time.
2. Although there are fine-scale differences in the $\Delta\delta^{18}O$ records between this site and that in the Andaman Sea [see *Stoll et al*., 2007a], the coherence of these records on $\gg$ka timescales shows that cores in both locations are recording the same overall changes in precipitation, even if the focus of that precipitation shifts over time with movement of the ITCZ.
3. A change in end-member $\delta^{18}O_{freshwater}$ of the magnitude of that predicted by modeling translates into relatively small errors in $\Delta\delta^{18}O$-derived freshwater flux reconstructions (see below).
4. The magnitude of the Ba/Ca_{sw} excursion between 68 and 49 ka is not inconsistent with that derived from $\Delta\delta^{18}O$. An MIS4/3 Arakan/Irrawaddy low-salinity end-member [Ba] within the range of that observed for other river systems (Figure 5) would put absolute freshwater flux estimates from the two proxies in agreement. This may be tested if Ba_{sw} data proximal to the Arakan and Irrawaddy become available.

In summary, the broad coherence of freshwater flux calculations over the past derived from both foraminifera Ba/Ca and $\delta^{18}O$ imply that residual oxygen isotopes track broad changes in freshwater flux in the Bay of Bengal on timescales greater than a thousand years. Because the $\Delta\delta^{18}O$ records between this site and the Andaman Sea show a similar trend on long timescales, our freshwater record from this site must relate to broad changes in monsoon rainfall, even if the focus of precipitation shifted to the east during colder intervals [*Stoll et al*., 2007a; *Pausata et al*., 2011].

4.2. The Relationship Between Freshwater Flux and Other Monsoon Indices

Assuming that the Arabian Sea summer-monsoon (ASM) factor [*Clemens and Prell*, 2003] can be related consistently to relative changes in ISM intensity over time (i.e., that two time intervals with the same factor were characterized by an equally intense monsoon), then the increase in monsoon intensity seen in all records shortly before the MIS 4/3 boundary (Figure 6) represents one of the strongest monsoons at any point over the last two glacial-interglacial cycles.

Our record differs from those previously published in that it is directly related to the amount of freshwater entering the Bay of Bengal and therefore uniquely offers a constraint of the amount of precipitation and meltwater draining through the Ganges-Brahmaputra and other river systems through time. In contrast, ISM records based on upwelling/vertical mixing-sensitive proxies such as $\delta^{15}N$ and biogenic opal production [*Clemens and Prell*, 2003] or *G. ruber-N. dutertrei* $\Delta\delta^{18}O$ [*Bolton et al*., 2013] give an indication of the strength of the winds resulting from the pressure differential between the Indian Ocean and south Asia landmass, but do not directly relate to the amount or composition of the precipitation that the monsoon delivers to the Indian subcontinent, southern China and Burma. However, whilst we report the first

quantitative estimates of freshwater volume draining into the Bay of Bengal, our record does not enable us to independently assess secular shifts in the bulk isotopic and elemental composition of this freshwater end-member.

Over the last deglaciation, the $\Delta\delta^{18}O$ records shown in Figure 6f deviate from ISM stacks and speleothem $\delta^{18}O$ data [e.g., *Wang et al*., 2008]. These data sets broadly correlate with northern hemisphere summer insolation, which has long been recognized as one of the major components of monsoon strength forcing [e.g., *Overpeck et al*., 1996], albeit with a lag between proxy monsoon strength and precession minima [*Caley et al*., 2011a; *Bolton et al*., 2013]. There are multiple lines of evidence for enhanced monsoon intensity through the 65°N insolation increase between 20 and 10 ka: Chinese speleothems [*Wang et al*., 2008], Indian Ocean stratification [*Bolton et al*., 2013], wind proxy stacks (Figures 6c and 6d), properties of the sediment deposited on the Chinese Loess Plateau [e.g., *Liu and Ding*, 1998], and sediment accumulation rates on the Bengal Fan [*Goodbred and Kuehl*, 2000]. Assuming that precipitation volume and monsoon intensity are closely linked, the central-western Bay of Bengal $\Delta\delta^{18}O$ record (Figure 6f) would appear to contradict these reconstructions. Given the unequivocal nature of the accumulated evidence for a greater than present-day Holocene monsoon, this implies one or a combination of: (1) far less or no freshwater flux to the western Bay of Bengal, (2) differential evaporation rates across the Bay of Bengal, or (3) a freshwater component with a substantially different (positive) $\delta^{18}O$. Given the implausible nature of the latter (requiring a $>6‰$ $\delta^{18}O$ compositional shift in the freshwater end-member), and that there is good evidence for the first of these scenarios [*Duplessy*, 1982; *Stoll et al*., 2007a], we interpret the relationship between our freshwater flux reconstruction and previous monsoon indices (Figures 6f and 6g) in the context of a shift of the focus of precipitation through time.

Whilst the $\Delta\delta^{18}O$ record derived from the data of *Rashid et al*. [2011] suggest that the intense Holocene monsoon was not manifest in the western Bay of Bengal [see also *Mahesh and Banakar*, 2014], it is important to note that the Holocene is not represented in our record. Neither our Ba/Ca data point (from the Younger Dryas) or the $\delta^{18}O$ data [*Stoll et al*., 2007a] are of sufficient resolution to capture the magnitude or timing or post-LGM changes in freshwater flux. Therefore, our record does not necessarily imply that there was no freshwater flux to the central Bay of Bengal since the LGM. Specifically, Figure 6f is dominated by the western part of the bay between ~20 and 0 ka, which was characterized by a negligible freshwater component. This is not representative of overall monsoon intensity or monsoon rainfall over this interval.

4.3. Spatial Patterns in Bay of Bengal Freshwater Flux

Previous monsoon stacks and records derived from wind-sensitive proxies [*Caley et al*., 2011a; *Clemens and Prell*, 2003; *Bolton et al*., 2013] and high-resolution data from Chinese speleothems [e.g., *Wang et al*., 2008] imply a similar rapid increase in monsoon intensity during T1 and shortly prior to the MIS4/3 boundary at around 59.8 ka [*Liu et al*., 2010]. Assuming that our freshwater record is related to monsoon precipitation (summer All India monsoon Rainfall—AIR) [*Parthasarathy et al*., 1995; *Goswami et al*., 2006b] irrespective of a potential shift of the ITCZ, there must be a fundamental difference between these two climatic transitions which appear to be characterized by similar shifts in wind strength but very different sources and fluxes of freshwater to the central Bay of Bengal. The spatial distribution of freshwater flux to the Bay of Bengal over the last 70 ka is shown in Figure 7, based on $\Delta\delta^{18}O$ for all sites for which data are available over this time. An error of $\pm1‰$ in $\delta^{18}O_{freshwater}$ and 2°C (to account for potential ΔT between any given site and ODP Site 758) have been added to $\Delta\delta^{18}O$-derived freshwater flux reconstructions. A $\delta^{18}O_{freshwater}$ error of this magnitude is equivalent to that which may be expected from either changes in precipitation [*Marzin et al*., 2013; *Pausata et al*., 2011] or greater than present-day meltwater contribution (section 4.1.2).

Calculated freshwater components derived from *Kudrass et al*. [2001] from the northernmost Bay of Bengal (Figure 7) and the Andaman Sea [*Colin et al*., 1999] show that the Holocene was characterized by a much greater freshwater flux through both the Ganges-Brahmaputra and Irrawaddy systems. As we argue above, the fact that this is not observed at VM29-19 [*Rashid et al*., 2011]—a core further to the west—confirms previous evidence that precipitation broadly shifted toward the east [*Colin et al*., 1999; *Stoll et al*., 2007a]; the west Bay of Bengal record [*Rashid et al*., 2011] is too distal to be affected by freshwater during these times, whereas our Ba/Ca and the $\Delta\delta^{18}O$ record from RC12–343 in the central-east Bay of Bengal does not cover the Holocene in sufficient resolution. The LGM was characterized by overall lower freshwater fluxes through both drainage systems and a shift in the Bay of Bengal gradient from N-S to E-W [*Duplessy*, 1982]; additional

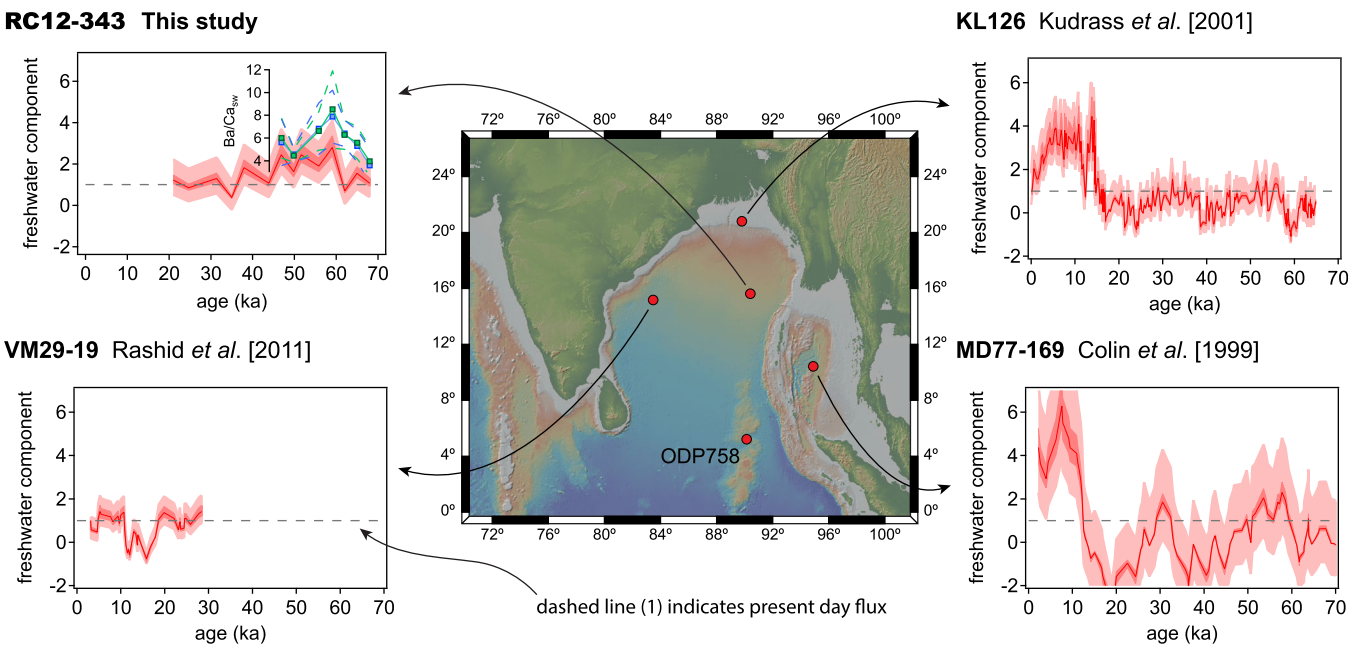

Figure 7. Spatiotemporal variation in $\Delta\delta^{18}$O-derived freshwater flux to the Bay of Bengal, with RC12–343 Ba/Ca_{sw} shown for comparison. All oxygen isotope data are normalized to present day so that a freshwater component of 1 represents an equivalent freshwater flux to a given core site compared to today. All $\Delta\delta^{18}$O data are calculated relative to IODP Site 758 and assume equivalent temperature evolution, with the exception of MD77–169 for which the $\Delta\delta^{18}$O record is as originally published [*Colin et al.*, 1999, relative to SHI90-14, Banda Sea], as primary foraminifera δ^{18}O data were not reported. Inner (dark red) error bands represent an uncertainty in $\delta^{18}O_{freshwater}$ of $\pm 1‰$; outer (light red) error bands represent a temperature offset between a given site and that used to normalize δ^{18}O of ± 1°C. The outer error band has been applied additively to the inner band and can therefore be considered representative of maximum error provided deviation from these modern assumptions was no greater than this. Bathymetry and topography data are from *Ryan et al.* [2009].

evidence exists that T1 marks the start of significant freshwater leakage to the Arabian Sea [*Mahesh and Banakar*, 2014]. The MIS4/3 transition (~65–55 ka) is characterized by greater than present freshwater flux to the Bay of Bengal, although the KL126 $\Delta\delta^{18}$O record (Figure 7) and the ϵNd data at RC12–343 [*Stoll et al.*, 2007a; *Kudrass et al.*, 2001] show that this freshwater must have been sourced largely from the Irrawaddy and/or the Arakan drainage system, in contrast to the mid-Holocene.

Overall, these data taken together (Figure 7) suggest that the monsoon stacks and other indicators of wind strength in the evaporative source region of the ISM (e.g., the sediment total reflectance record of *Deplazes et al.* [2014]) broadly relate to the magnitude of ISM precipitation and that insolation-driven changes in monsoon intensity are also observed in precipitation flux records. However, Arabian Sea productivity records are closely related to North Atlantic climate (D-O) oscillations and Heinrich events [*Deplazes et al.*, 2014; *Ziegler et al.*, 2010; *Reichart et al.*, 2004], whereas there is no consistent link between freshwater flux and productivity/stratification. Even though most freshwater flux records are not of sufficient resolution to assess rapid response to north-Atlantic forcing (Figure 7), with the exception of that of *Kudrass et al.* [2001], there are evidently large shifts in freshwater flux through time which are not only or principally controlled by Arabian Sea wind strength.

Given that the strength of the ISM is at present largely driven by the pressure differential arising from sensible and latent heating of and above Asia compared to the tropical ocean, the latter derived from tropospheric condensation of vapor originating in the Arabian Sea and Indian Ocean [*Webster*, 1994; *Clemens and Prell*, 2003], it may be expected that the intensity of the ISM is—aside from other forcings (Atlantic Meridional Overturning Circulation (AMOC); North Atlantic Oscillation (NAO) etc.)—driven by the difference in solar insolation between the Asian landmass and equatorial ocean [*Webster*, 1994]. However, previous studies have shown that shifts in monsoon intensity cannot simply relate to changes in northern hemisphere insolation (i.e., heating of the Asian landmass), partly because of the simple observation that monsoon records lag precession minima (maximum northern hemisphere summer insolation) [e.g., *Clemens and Prell*, 2003; *Bolton et al.*, 2013]. A stack of freshwater flux records from the Bay of Bengal (Figure 8) lags insolation maxima by ~4 ka and demonstrates that this is also the case for monsoon rainfall. The potential role of northern hemisphere-equatorial differences in summer insolation has been previously recognized by *Saraswat et al.* [2012], who proposed the

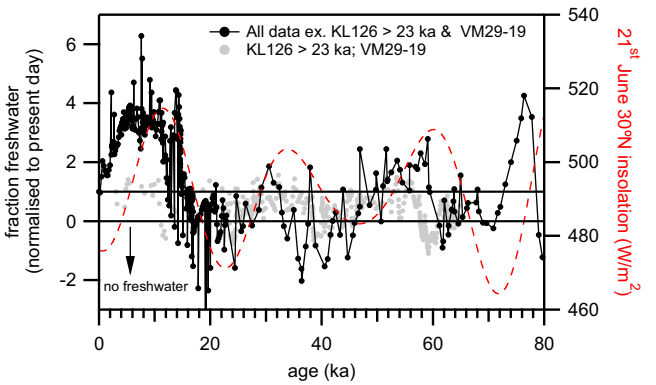

Figure 8. Stacked freshwater flux data (from Figure 7) and its relationship to 21 June 30°N insolation variation over the past 80 ka. Data >23 ka from site KL126 is shown in grey because this site is insensitive to freshwater over this intervals as precipitation shifted toward the east (see text for details). All data from VM29-19 are omitted as this site is distal from any major freshwater source over the past 80 ka.

insolation gradient as the dominant force driving monsoon intensity. Mechanistically this may explain shifts in monsoon precipitation because large insolation gradients can be expected to result in a greater pressure differential, driving winds and moisture transport to the Asian landmass. However, this cannot explain the lag between our freshwater flux calculations and maxima in the 30°N-equator insolation gradient.

In order to explain the orbital timing of our freshwater stack (Figure 8), we examine the fundamental mechanisms which drive the ISM at present. Figure 9a shows insolation curves for May–July at the equator (energy to the source region of summer monsoon precipitation), June–July at 30°N (heating of the Asian landmass) and the average June–July difference in insolation between 30°N and the equator (a proxy for the magnitude of the pressure differential between the source region and Eurasia, which drives the ISM winds). Superimposed on these curves are lines that define the position of freshwater flux maxima from our freshwater stack, from Figure 8. We propose that these maxima relate to the insolation curves in the following way, as a result of three fundamental processes that control the intensity and the length of ISM precipitation. (1) Insolation to the evaporative source region. Maximum SST in the western equatorial Indian Ocean occurs in May [*Locarnini et al*., 2013] and freshwater maxima occur at points at which there is no decrease in insolation from May through to July. Because the proportion of energy that goes into latent and sensible heat greatly increases as SST rises above 28°C [*Priestley*, 1966], the amount of vapor transported from the equatorial Indian Ocean is likely to be greatly sensitive to changes in insolation over these months and therefore manifest in AIR. (2) Insolation to the Asian landmass. The lines defining freshwater maxima occur at times when there is no or little decrease in insolation between June and July at 30°N. (3) The summer insolation gradient between the Asian landmass and the equatorial Indian Ocean. Larger freshwater fluxes (at ~8 and 58 ka) occur close to maxima in this gradient.

Insolation curves which relate to these three processes are shown in Figure 9b, and are normalized in Figure 9c ($z_i = \frac{x_i - \mu}{\sigma}$). The curves were then variably weighted and combined in order to produce a freshwater forcing curve (Figure 9d), which most closely matches the freshwater stack when a fractional importance of 0.45 is assigned to the curve that relates to the 30°N-equator summer insolation gradient. Because the remaining two processes (1 and 2 above) produce forcing curves that are almost identical (Figure 9c), it is not possible to assess the relative contribution of each. Maximum freshwater flux to the Bay of Bengal therefore occurs when these three processes act to evaporate and transport the greatest volume of water. This model is capable of almost exactly reproducing the orbital timing of monsoon-driven peak freshwater flux to the Bay of Bengal as well as secular variation in the magnitude of freshwater flux. The importance of equatorial surface ocean heating on AIR, before the onset of the monsoon season, has been recognized "summer monsoon winds are established in May" [*Clemens et al*., 2010]. This explains the importance of latent energy to the evaporative source region before the ISM season, even though transport time of moisture from the equator to the precipitation region is relatively much shorter [*Breitenbach et al*., 2010]. It is sustained and prolonged periods of latent heating of the ocean which results in longer monsoons, coupled with a relatively large insolation gradient driving the efficiency of air mass transport to Asia. Finally, prolonged and constant high insolation at 30°N enables a longer monsoon (process 2), which is a plausible driver of monsoon intensity on kiloannus timescales given that modern instrumental data show that years characterized by above average AIR are principally driven by an extension of the positive tropospheric temperature anomaly though September [*Goswami et al*., 2006b].

The relationship between insolation and the precipitation forcing curve shown in Figure 9d breaks down during minima (e.g., 60–70 ka) because a certain threshold is required for some freshwater to be present at

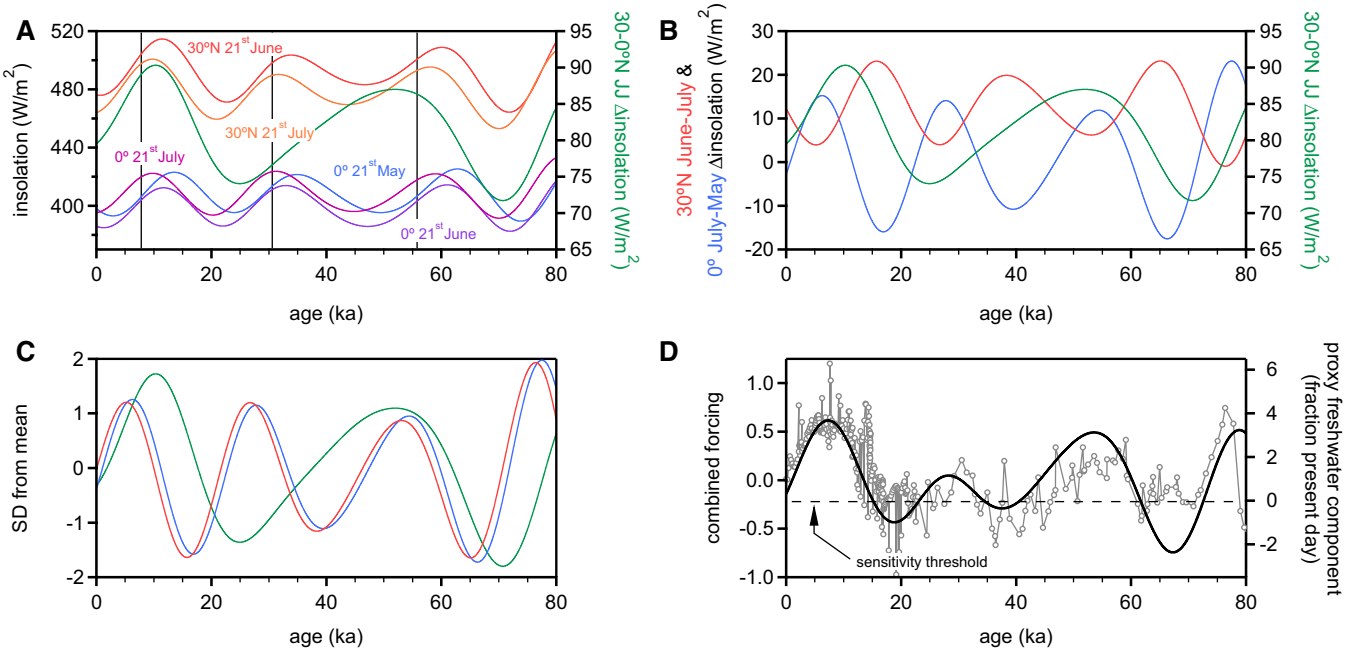

Figure 9. (A) Insolation curves for 30°N and the equator through May–July and the average 21st June to 21st July insolation difference between 30°N and the equator. The vertical lines indicate the timings of maxima in freshwater flux to the Bay of Bengal from our stacked freshwater record (Figure 8). These lag 21st June insolation maxima but occur at times when there is an increase in insolation at the equator from May to July and there is little decrease in insolation at 30°N between June and July. (b) Isolating the main components that control Bay of Bengal freshwater flux: red—the decrease in insolation at 30°N between June and July (minimum = positive forcing), blue—increase in insolation from May to July at the equator (maximum = positive forcing), green—mean summer 30°N-equator insolation difference (higher = positive forcing), see text for details. (c) Normalized curves from Figure 9b. (d) A combined forcing curve based on the curves shown in Figure 9c with 45% weighting assigned to the summer insolation gradient between 30°N and the equator (green line in Figure 9c). The other forcings act with the same magnitude and almost the same timing and the relative importance of each cannot be identified. This combined forcing curve accurately matches the timing of peaks in freshwater flux.

the core sites, which are mostly not coastal proximal. Our data and calculations derived from previously published data enable this threshold to be approximately estimated (Figure 9d): it occurs slightly below present day forcing (−0.22). Below this threshold, a freshwater flux of ∼0 is observed at the nonproximal core sites which become insensitive to precipitation shifts, although this is not the case for the proximal core site [*Kudrass et al*., 2001] which appears to accurately reflect fine-scale changes throughout the last 80 ka, albeit with a sensitivity which cannot be related to orbital forcing given that the focus of precipitation must have shifted through time. For this purpose nonproximal core sites are required (such as RC12–343), which are sensitive to freshwater from more than one drainage basin.

4.4. Mechanisms for an Intense Indian Monsoon Around MIS4/3

We argue above that AIR is closely related to two or three processes that affect the May–July latent heating of the equatorial surface ocean, the length of sustained high insolation to the low-mid latitude northern hemisphere and the summer insolation gradient between these locations. The intense monsoon that occurred around the MIS4/3 transition (Figures 6 and 8) is therefore explicable by this gradient and is only characterized by a smaller change in freshwater flux than the LGM to the Holocene because the insolation gradient at 68 ka is below the threshold at which a freshwater signature relating proportionally to orbital forcing can be expected at the Bay of Bengal core sites that we discuss (Figure 9d). This mechanism may also explain the relatively short (∼3 ka) lag between precession and δ^{18}O minima observed in Chinese speleothems [*Caley et al*., 2011a]. This is because the same fundamental processes control AIR and aspects of Chinese speleothem δ^{18}O, namely energy transferred to latent heating at the source region controlled by low-latitude insolation, and the Asian landmass-Indian Ocean pressure differential which transports air masses with an efficiency controlled by the insolation gradient. However, the importance of winter monsoon processes for these eastern cave records must also be recognized [*Clemens et al*., 2010] as well as the amount of precipitation recycling that occurs before water vapor is transported to these sites [*Pausata et al*., 2011].

On (sub)ka timescales, the ISM is substantially more complex than to simply be controlled by the two/three forcings that we identify above. There is good evidence that north Atlantic climate strongly impacts on Indian monsoon dynamics, in particular that Heinrich events and D-O oscillations controlled the position of the ITCZ, the temperature of and productivity in both the Arabian Sea and Indian Ocean, as well as the isotopic composition of cave carbonates to varying degrees [*Deplazes et al*., 2014; *Ziegler et al*., 2010; *Zhang and Delworth*, 2005; *Liu et al*., 2010; *Reichart et al*., 2004]. D-O oscillations have also been matched to $\delta^{18}O_{sw}$ at a site proximal to the Ganges-Brahmaputra delta [*Kudrass et al*., 2001] despite the fact that this core is too sensitive to local precipitation patterns to track AIR before the LGM. Evidently monsoon dynamics are controlled or modulated by different processes on different timescales. The Atlantic Multidecadal Oscillation (AMO) is statistically significantly correlated to AIR and anticorrelated with Niño3 SST over the last 140 years. This is thought to be through an atmospheric teleconnection which links periods of positive North Atlantic SST anomalies to a positive anomaly in the mean pressure difference between Eurasia and the equatorial Indian Ocean [*Goswami et al*., 2006b] and is a significant control even once the potential influence of the El Niño Southern Oscillation (ENSO) has been removed, although this is another source of multidecadal shifts in AIR [*Goswami and Xavier*, 2005]. The strong correlation between some monsoon indices and D-O and H-events [e.g., *Deplazes et al*., 2014] suggests that these are additional forcings. The mechanism for this is likely based in a strong teleconnection through changes in atmospheric pressure gradients and Atlantic circulation resulting from sudden north Atlantic SST warming, which may be explained in relation to AMOC [e.g., *Clark et al*., 2001] and/or ice shelf collapse [*Petersen et al*., 2013] and linked to AIR through a similar mechanism to the AMO [*Goswami et al*., 2006b; *Sun et al*., 2012]. Finally, the feedback between Himalayan ice-albedo and sensible heating of the Asian landmass has been suggested to play an important role in the close relationship between ISM proxy records and northern hemisphere climate oscillations [*Kudrass et al*., 2001], which may provide the necessary amplification by which D-O events are equally pronounced in tropical records. The relatively more frequent D-O oscillations during MIS3 may explain the offset between the freshwater flux proxy stack and the freshwater forcing curve (Figure 9d) over this time. However, it should also be borne in mind that $>$50% of the stack from this interval comes from a core in the Andaman Sea [*Colin et al*., 1999] which may bias the data set toward lower freshwater fluxes.

Whilst an alternative explanation for the timing of freshwater flux to the Bay of Bengal has been proposed to explain the lag between precession minima and Chinese speleothem $\delta^{18}O$ [*Clemens et al*., 2010], this cannot explain the similar lag observed in the freshwater flux record (Figure 8). Although 34% of annual precipitation arriving to the location of these speleothems is derived from the north between September–March [*Clemens et al*., 2010], this is not the case for freshwater entering the Bay of Bengal. It has also been noted that a common direct driving mechanism cannot explain the Arabian Sea monsoon records [*Bolton et al*., 2013]. Similarly, it may well be the case that several related but different mechanisms are required to explain the different forcings of the various AIR-sensitive proxy records.

On orbital timescales we argue that Indian monsoon rainfall is largely governed by the processes that we describe in section 4.3. Because the stack shown in Figure 8 is low-resolution throughout MIS3, it is not possible to assess the importance of northern-hemisphere D-O/H-events which are preserved in coastal proximal sites [*Kudrass et al*., 2001], whereas central Bay of Bengal cores may well be insensitive to more subtle changes in AIR. The rise in freshwater flux as shown by our Ba/Ca record between 70 and 60 ka despite this period containing H6 suggests a relatively minor control of major north Atlantic events on monsoon precipitation compared to the average summer 30°N-equator insolation gradient and other forcings described above. Finally, although the concept of a global monsoon has been disputed [*Caley et al*., 2011b] and whilst monsoons in different parts of the globe are highly likely to be differentially influenced by regional-global climate forcings, we note the high coherence of our Bay of Bengal freshwater stack and the Ba/Ca record for the Gulf of Guinea [*Weldeab et al*., 2007].

5. Conclusions

We reconstruct changes in temperature and freshwater flux to the central Bay of Bengal (core RC12–343) during MIS4/3 (68–45 ka), derived from laser-ablation depth-profiling of individual chambers of the surface-dwelling planktic foraminifera *G. ruber*. We demonstrate the importance of combined SEM-LA characterization of preservation, especially at sites characterized by high-organic carbon burial rates and consequently several

diagenetic styles (such as this), which are not always identifiable using geochemical signatures of preservation (e.g., Al-Mn/Ca). Complex preservation is likely to be common to many sites influenced by freshwater flux. Our analyses provide a method of obtaining useful palaeoceanic data from variably preserved samples and highlight the need for SEM images that show chamber wall microtexture. Based on the strong correlation between Ba/Ca and Y-REE/Ca ratios, we demonstrate that primary test Ba/Ca may be reconstructed from foraminifera that show elevated Ba/Ca as a result of diagenetic processes. Our Mg/Ca data indicate that the central Bay of Bengal was 2–3°C cooler during MIS4/3 than at present, with no resolvable temperature variation between 68–45 ka. However, Ba/Ca_{sw} reconstructions show high variability. The coherence of these estimates with that calculated from $\Delta\delta^{18}O$ of the same material (residual $\delta^{18}O$ compared to a nearby site with no freshwater influence), and with previous ISM stacks, demonstrate that our techniques for extracting primary geochemical information from variably preserved samples are effective and robust.

Our data demonstrate that Ba/Ca and $\Delta\delta^{18}O$-derived freshwater estimates produce consistent results through time, implying little bias in such records resulting from potential changes in the isotopic and elemental composition of freshwater, or secular shifts in the regional focus of precipitation. This enables us to produce a Bay of Bengal freshwater stack for the past 80 ka derived from previously published data sets [*Stoll et al*., 2007a; *Colin et al*., 1999; *Kudrass et al*., 2001; *Chen and Farrell*, 1991] that enables the orbital timing of monsoon precipitation shifts to be examined. This record is not sensitive to pre-Holocene changes in the focus of precipitation to the East [e.g., *Pausata et al*., 2011] because these eastern drainage systems also ultimately transport freshwater to the Bay of Bengal and Andaman Sea.

Finally, we develop a freshwater forcing curve based on a combination of two or three factors that are known to control ISM dynamics at present: (1) constant or increasing insolation to the equatorial Indian Ocean and Arabian Sea between May and July, controlling latent heating of the surface ocean in the moisture source region, (2) constant or increasing 30°N insolation between June and July, controlling the seasonal longevity of the low-pressure system over Asia, and (3) the summer insolation gradient between 30°N and the equator which drives air masses toward India-Bangladesh. Our freshwater stack lags precession minima by 3–4 ka but a forcing curve constructed from these parameters can entirely explain the timing of freshwater flux maxima to the Bay of Bengal, implying a relatively minor control of sudden North Atlantic climate events such as D-O cycles and Heinrich events to large-scale shifts in freshwater flux. Given that it is evident that North Atlantic events strongly influence proxies that are dominantly controlled by wind strength and/or productivity [e.g., *Deplazes et al*., 2014], it is possible that more high-resolution data [e.g., *Kudrass et al*., 2001] may show that NAO and/or AMOC play a greater role in controlling fine-scale shifts in freshwater flux than is presently apparent, although monsoon rainfall amount is controlled to a greater extent by seasonal and latitudinal insolation gradients.

Acknowledgments
D.E. acknowledges a NERC postgraduate studentship at RHUL. We would like to thank Tomasz Goral and Alex Ball at the NHM London for help with SEM imaging. Data policy compliance: All new data presented in this paper are available in Table 1 and in supporting information. The authors gratefully acknowledge the constructive comments of two anonymous reviewers.

References

Andersen, K. K., et al. (2004), High-resolution record of Northern Hemisphere climate extending into the last interglacial period, *Nature*, *431*(7005), 147–151.

Barker, S., M. Greaves, and H. Elderfield (2003), A study of cleaning procedures used for foraminiferal Mg/Ca paleothermometry, *Geochem. Geophys. Geosyst.*, *4*(9), 8407, doi:10.1029/2003GC000559.

Barrows, T. T., and S. Juggins (2005), Sea-surface temperatures around the Australian margin and Indian Ocean during the Last Glacial Maximum, *Quat. Sci. Rev.*, *24*(7), 1017–1047.

Bolton, C. T., et al. (2013), A 500,000 year record of Indian summer monsoon dynamics recorded by eastern equatorial Indian Ocean upper water-column structure, *Quat. Sci. Rev.*, *77*, 167–180.

Bond, G. C., W. Showers, M. Elliot, M. Evans, R. Lotti, I. Hajdas, G. Bonani, and S. Johnson (1999), The North Atlantic's 1–2 kyr climate rhythm: Relation to Heinrich events, Dansgaard/Oeschger cycles and the little ice age, *Geophys. Monogr. Ser.*, *112*, 35–58.

Breitenbach, S. F., J. F. Adkins, H. Meyer, N. Marwan, K. K. Kumar, and G. H. Haug (2010), Strong influence of water vapor source dynamics on stable isotopes in precipitation observed in Southern Meghalaya, NE India, *Earth Planet. Sci. Lett.*, *292*(1), 212–220.

Caley, T., B. Malaizé, S. Zaragosi, L. Rossignol, J. Bourget, F. Eynaud, P. Martinez, J. Giraudeau, K. Charlier, and N. Ellouz-Zimmermann (2011a), New Arabian Sea records help decipher orbital timing of Indo-Asian monsoon, *Earth Planet. Sci. Lett.*, *308*(3), 433–444.

Caley, T., B. Malaizé, M. Revel, E. Ducassou, K. Wainer, M. Ibrahim, D. Shoeaib, S. Migeon, and V. Marieu (2011b), Orbital timing of the Indian, East Asian and African boreal monsoons and the concept of a global monsoon, *Quat. Sci. Rev.*, *30*(25), 3705–3715.

Carroll, J., et al. (1993), The role of the Ganges-Brahmaputra mixing zone in supplying barium and ^{226}Ra to the Bay of Bengal, *Geochim. Cosmochim. Acta*, *57*(13), 2981–2990.

Chen, M.-T., and J. Farrell (1991), Planktonic foraminifer faunal variations in the northeastern Indian ocean: A high-resolution record of the past 800,000 years from site 758, in *Proceedings of Ocean Drilling Program Science Results*, vol. 121, edited by J. Weissel, et al., Ocean Drilling Program, College Station, TX, pp. 125–140.

Clark, P. U., S. J. Marshall, G. K. Clarke, S. W. Hostetler, J. M. Licciardi, and J. T. Teller (2001), Freshwater forcing of abrupt climate change during the last glaciation, *Science*, *293*(5528), 283–287.

Clemens, S. C., and W. L. Prell (2003), A 350,000 year summer-monsoon multi-proxy stack from the Owen Ridge, Northern Arabian Sea, *Mar. Geol.*, *201*(1), 35–51.
Clemens, S. C., W. L. Prell, and Y. Sun (2010), Orbital-scale timing and mechanisms driving Late Pleistocene Indo-Asian summer monsoons: Reinterpreting cave speleothem δ^{18}O, *Paleoceanography*, *25*, PA4207, doi:10.1029/2010PA001926.
Coffey, M., F. Dehairs, O. Collette, G. Luther, T. Church, and T. Jickells (1997), The behaviour of dissolved barium in estuaries, *Estuarine Coastal Shelf Sci.*, *45*(1), 113–121.
Colin, C., L. Turpin, J. Bertaux, A. Desprairies, and C. Kissel (1999), Erosional history of the Himalayan and Burman ranges during the last two glacial–interglacial cycles, *Earth Planet. Sci. Lett.*, *171*(4), 647–660.
Creech, J., J. Baker, C. Hollis, H. Morgans, and E. Smith (2010), Eocene sea temperatures for the mid-latitude southwest Pacific from Mg/Ca ratios in planktonic and benthic foraminifera, *Earth Planet. Sci. Lett.*, *299*, 483–495.
Delaygue, G., E. Bard, C. Rollion, J. Jouzel, M. Stiévenard, J.-C. Duplessy, and G. Ganssen (2001), Oxygen isotope/salinity relationship in the northern Indian Ocean, *J. Geophys. Res.*, *106*(C3), 4565–4574.
Deplazes, G., A. Lückge, J.-B. W. Stuut, J. Pätzold, H. Kuhlmann, D. Husson, M. Fant, and G. H. Haug (2014), Weakening and strengthening of the Indian monsoon during Heinrich events and Dansgaard-Oeschger oscillations, *Paleoceanography*, *29*, 99–114, doi:10.1002/2013PA002509.
Duplessy, J. C. (1982), Glacial to interglacial contrasts in the northern Indian Ocean, *Nature*, *295*, 494–498.
Edmond, J., E. Boyle, D. Drummond, B. Grant, and T. Mislick (1978), Desorption of barium in the plume of the Zaire (Congo) River, *Neth. J. Sea Res.*, *12*(3), 324–328.
Eggins, S., P. De Deckker, and J. Marshall (2003), Mg/Ca variation in planktonic foraminifera tests: Implications for reconstructing palaeo-seawater temperature and habitat migration, *Earth Planet. Sci. Lett.*, *212*(3-4), 291–306.
Elderfield, H., and G. Ganssen (2000), Past temperature and δ^{18}O of surface ocean waters inferred from foraminiferal Mg/Ca ratios, *Nature*, *405*, 442–445.
Erez, J., and B. Luz (1983), Experimental paleotemperature equation for planktonic foraminifera, *Geochim. Cosmochim. Acta*, *47*(6), 1025–1031.
Evans, D., and W. Müller (2013), LA-ICPMS elemental imaging of complex discontinuous carbonates: An example using large benthic foraminifera, *J. Anal. At. Spectrosc.*, *28*, 1039–1044, doi:10.1039/c3ja50053e.
Evans, D., J. Erez, S. Oron, and W. Müller (2015), Mg/Ca-temperature and seawater-test chemistry relationships in the shallow-dwelling large benthic foraminifera *Operculina ammonoides*, *Geochim. Cosmochim. Acta*, *148*, 325–342.
Fehrenbacher, J. S., and P. A. Martin (2014), Exploring the dissolution effect on the intrashell Mg/Ca variability of the planktic foraminifer *Globigerinoides ruber*, *Paleoceanography*, *29*, 854–868, doi:10.1002/2013PA002571.
Francois, R., S. Honjo, R. Krishfield, and S. Manganini (2002), Factors controlling the flux of organic carbon to the bathypelagic zone of the ocean, *Global Biogeochem. Cycles*, *16*(4), 1087, doi:10.1029/2001GB001722.
Frey, H., H. Machguth, M. Huss, C. Huggel, S. Bajracharya, T. Bolch, A. Kulkarni, A. Linsbauer, N. Salzmann, and M. Stoffel (2014), Estimating the volume of glaciers in the Himalayan–Karakoram region using different methods, *The Cryosphere*, *8*, 2313–2333, doi:10.5194/tc-8-2313-2014.
Goodbred, S. L., and S. A. Kuehl (2000), Enormous Ganges-Brahmaputra sediment discharge during strengthened early holocene monsoon, *Geology*, *28*(12), 1083–1086.
Goswami, B. N., and P. K. Xavier (2005), ENSO control on the south Asian monsoon through the length of the rainy season, *Geophys. Res. Lett.*, *32*, L18717, doi:10.1029/2005GL023216.
Goswami, B. N., V. Krishnamurthy, and H. Annmalai (1999), A broad-scale circulation index for the interannual variability of the Indian summer monsoon, *Q. J. R. Meteorol. Soc.*, *125*(554), 611–633.
Goswami, B. N., V. Venugopal, D. Sengupta, M. Madhusoodanan, and P. K. Xavier (2006a), Increasing trend of extreme rain events over India in a warming environment, *Science*, *314*(5804), 1442–1445.
Goswami, B. N., M. Madhusoodanan, C. Neema, and D. Sengupta (2006b), A physical mechanism for north Atlantic SST influence on the Indian summer monsoon, *Geophys. Res. Lett.*, *33*, L02706, doi:10.1029/2005GL024803.
Guptha, M., W. Curry, V. Ittekkot, and A. Muralinath (1997), Seasonal variation in the flux of planktic foraminifera; Sediment trap results from the Bay of Bengal, northern Indian Ocean, *J. Foraminiferal Res.*, *27*(1), 5–19.
Hall, J. M., and L.-H. Chan (2004), Ba/Ca in *Neogloboquadrina pachyderma* as an indicator of deglacial meltwater discharge into the western Arctic Ocean, *Paleoceanography*, *19*, PA1017, doi:10.1029/2003PA000910.
Hanor, J. S., and L.-H. Chan (1977), Non-conservative behavior of barium during mixing of Mississippi River and Gulf of Mexico waters, *Earth Planet. Sci. Lett.*, *37*(2), 242–250.
Hollis, C., et al. (2009), Tropical sea temperatures in the high-latitude South Pacific during the Eocene, *Geology*, *37*(2), 99–102.
Hönisch, B., K. Allen, A. Russell, S. Eggins, J. Bijma, H. Spero, D. Lea, and J. Yu (2011), Planktic foraminifers as recorders of seawater Ba/Ca, *Mar. Micropaleontol.*, *79*(1), 52–57.
Ittekkot, V., R. Nair, S. Honjo, V. Ramaswamy, M. Bartsch, S. Manganini, and B. Desai (1991), Enhanced particle fluxes in Bay of Bengal induced by injection of fresh water, *Nature*, *351*(6325), 385–387.
Jochum, K., et al. (2006), MPI-DING reference glasses for in situ microanalysis: New reference values for element concentrations and isotope ratios, *Geochem. Geophys. Geosyst.*, *7*, Q02008, doi:10.1029/2005GC001060.
Jochum, K., et al. (2011), Determination of reference values for NIST SRM 610–617 glasses following ISO guidelines, *Geostand. Geoanal. Res.*, *35*(4), 397–429, doi:10.1111/j.1751-908X.2011.00120.x.
Joung, D., and A. M. Shiller (2014), Dissolved barium behavior in Louisiana Shelf waters affected by the Mississippi/Atchafalaya River, *Geochim. Cosmochim. Acta*, *141*, 303–313.
Kisakürek, B., A. Eisenhauer, F. Bohm, D. Garbe-Schönberg, and J. Erez (2008), Controls on shell Mg/Ca and Sr/Ca in cultured planktonic foraminiferan, *Globigerinoides ruber* (white), *Earth Planet. Sci. Lett.*, *273*(3-4), 260–269.
Klaas, C., and D. E. Archer (2002), Association of sinking organic matter with various types of mineral ballast in the deep sea: Implications for the rain ratio, *Global Biogeochem. Cycles*, *16*(4), 1116, doi:10.1029/2001GB001765.
Kozdon, R., D. Kelly, N. Kita, J. Fournelle, and J. Valley (2011), Planktonic foraminiferal oxygen isotope analysis by ion microprobe technique suggests warm tropical sea surface temperatures during the Early Paleogene, *Paleoceanography*, *26*, PA3206, doi:10.1029/2010PA002056.
Kudrass, H., A. Hofmann, H. Doose, K. Emeis, and H. Erlenkeuser (2001), Modulation and amplification of climatic changes in the Northern Hemisphere by the Indian summer monsoon during the past 80 ky, *Geology*, *29*(1), 63–66.
Lea, D. W., and H. J. Spero (1994), Assessing the reliability of paleochemical tracers: Barium uptake in the shells of planktonic foraminifera, *Paleoceanography*, *9*(3), 445–452.

Li, Y.-H. (1982), A brief discussion on the mean oceanic residence time of elements, *Geochim. Cosmochim. Acta*, *46*(12), 2671–2675.
Lisiecki, L. E., and M. E. Raymo (2005), A Pliocene-Pleistocene stack of 57 globally distributed benthic δ^{18}o records, *Paleoceanography*, *20*, PA1003, doi:10.1029/2004PA001071.
Liu, D., et al. (2010), Sub-millennial variability of Asian monsoon intensity during the early MIS 3 and its analogue to the ice age terminations, *Quat. Sci. Rev.*, *29*(9), 1107–1115.
Liu, T., and Z. Ding (1998), Chinese loess and the paleomonsoon, *Annu. Rev. Earth Planet. Sci.*, *26*(1), 111–145.
Locarnini, R., et al. (2013), Volume 1: Temperature, *World Ocean Atlas 2013*, edited by S. Levitus, vol. 73, 40 pp., NOAA Atlas NESDIS, Md.
Mahesh, B., and V. Banakar (2014), Change in the intensity of low-salinity water inflow from the Bay of Bengal into the Eastern Arabian Sea from the Last Glacial Maximum to the Holocene: Implications for monsoon variations, *Palaeogeogr. Palaeoclimatol. Palaeoecol.*, *397*, 31–37.
Marzin, C., N. Kallel, M. Kageyama, J.-C. Duplessy, and P. Braconnot (2013), Glacial fluctuations of the Indian monsoon and their relationship with North Atlantic climate: New data and modelling experiments, *Clim. Past*, *9*(5), 2135–2151.
McCulloch, M., S. Fallon, T. Wyndham, E. Hendy, J. Lough, and D. Barnes (2003), Coral record of increased sediment flux to the inner Great Barrier Reef since European settlement, *Nature*, *421*(6924), 727–730.
Moore, W. S. (1997), High fluxes of radium and barium from the mouth of the Ganges-Brahmaputra River during low river discharge suggest a large groundwater source, *Earth Planet. Sci. Lett.*, *150*(1), 141–150.
Moore, W. S. (2010), The effect of submarine groundwater discharge on the ocean, *Annu. Rev. Mar. Sci.*, *2*, 59–88.
Müller, W., M. Shelley, P. Miller, and S. Broude (2009), Initial performance metrics of a new custom–designed ArF excimer LA–ICPMS system coupled to a two-volume laser–ablation cell, *J. Anal. At. Spectrom.*, *24*(2), 209–214.
Overpeck, J., D. Anderson, S. Trumbore, and W. Prell (1996), The southwest Indian Monsoon over the last 18000 years, *Clim. Dyn.*, *12*(3), 213–225.
Palmer, M. (1985), Rare earth elements in foraminifera tests, *Earth Planet. Sci. Lett.*, *73*(2), 285–298.
Parthasarathy, B., A. Munot, and D. Kothawale (1995), *Monthly and Seasonal Rainfall Series for All-India Homogeneous Regions and Meteorological Subdivisions, 1871–1994*, Indian Inst. of Trop. Meteorol., Pune, India.
Pausata, F. S., D. S. Battisti, K. H. Nisancioglu, and C. M. Bitz (2011), Chinese stalagmite δ^{18}O controlled by changes in the Indian monsoon during a simulated Heinrich event, *Nat. Geosci.*, *4*(7), 474–480.
Pearson, P. N., P. W. Ditchfield, J. Singano, K. G. Harcourt-Brown, C. J. Nicholas, R. K. Olsson, N. J. Shackleton, and M. A. Hall (2001), Warm tropical sea surface temperatures in the Late Cretaceous and Eocene epochs, *Nature*, *413*, 481–487.
Pena, L. D., E. Calvo, I. Cacho, S. Eggins, and C. Pelejero (2005), Identification and removal of Mn-Mg-rich contaminant phases on foraminiferal tests: Implications for Mg/Ca past temperature reconstructions, *Geochem. Geophys. Geosyst*, *6*, Q09P02, doi:10.1029/2005GC000930.
Petersen, S., D. Schrag, and P. U. Clark (2013), A new mechanism for Dansgaard-Oeschger cycles, *Paleoceanography*, *28*, 24–30, doi:10.1029/2012PA002364.
Pomiès, C., G. R. Davies, and S. M.-H. Conan (2002), Neodymium in modern foraminifera from the Indian Ocean: Implications for the use of foraminiferal Nd isotope compositions in paleo-oceanography, *Earth Planet. Sci. Lett.*, *203*(3), 1031–1045.
Priestley, C. (1966), The limitation of temperature by evaporation in hot climates, *Agric. Meteorol.*, *3*(3-4), 241–246.
Rashid, H., E. England, L. Thompson, and L. Polyak (2011), Late glacial to Holocene Indian summer monsoon variability based upon sediment records taken from the Bay of Bengal, *Terr. Atmos. Oceanic Sci.*, *22*(2), 215–228.
Regenberg, M., A. Regenberg, D. Garbe-Schönberg, and D. W. Lea (2014), Global dissolution effects on planktonic foraminiferal Mg/Ca ratios controlled by the calcite-saturation state of bottom waters, *Paleoceanography*, *29*, 127–142, doi:10.1002/2013PA002492.
Reichart, G.-J., F. Jorissen, P. Anschutz, and P. R. Mason (2003), Single foraminiferal test chemistry records the marine environment, *Geology*, *31*(4), 355–358.
Reichart, G.-J., H. Brinkhuis, F. Huiskamp, and W. J. Zachariasse (2004), Hyperstratification following glacial overturning events in the northern Arabian Sea, *Paleoceanography*, *19*, PA2013, doi:10.1029/2003PA000900.
Ryan, W. B., et al. (2009), Global multi-resolution topography synthesis, *Geochem. Geophys. Geosyst.*, *10*, Q03014, doi:10.1029/2008GC002332.
Saraswat, R., R. Nigam, S. Weldeab, A. Mackensen, and P. Naidu (2005), A first look at past sea surface temperatures in the equatorial Indian Ocean from Mg/Ca in foraminifera, *Geophys. Res. Lett.*, *32*, L24605, doi:10.1029/2005GL024093.
Saraswat, R., R. Nigam, A. Mackensen, and S. Weldeab (2012), Linkage between seasonal insolation gradient in the tropical northern hemisphere and the sea surface salinity of the equatorial Indian Ocean during the last glacial period, *Acta Geol. Sin.*, *86*, 1265–1275.
Saraswat, R., D. W. Lea, R. Nigam, A. Mackensen, and D. K. Naik (2013), Deglaciation in the tropical Indian Ocean driven by interplay between the regional monsoon and global teleconnections, *Earth Planet. Sci. Lett.*, *375*, 166–175.
Sarma, V. (2002), An evaluation of physical and biogeochemical processes regulating the oxygen minimum zone in the water column of the Bay of Bengal, *Global Biogeochem. Cycles*, *16*(4), 1099, doi:10.1029/2002GB001920.
Schmuker, B., and R. Schiebel (2002), Planktic foraminifers and hydrography of the eastern and northern Caribbean Sea, *Mar. Micropaleontol.*, *46*(3), 387–403.
Siderius, C., H. Biemans, A. Wiltshire, S. Rao, W. Franssen, P. Kumar, A. Gosain, M. van Vliet, and D. Collins (2013), Snowmelt contributions to discharge of the Ganges, *Sci. Total Environ.*, *468*, S93–S101.
Singh, S. P., S. K. Singh, and R. Bhushan (2013), Internal cycling of dissolved barium in water column of the Bay of Bengal, *Mar. Chem.*, *154*, 12–23.
Stoll, H. M., D. Vance, and A. Arevalos (2007a), Records of the Nd isotope composition of seawater from the Bay of Bengal: Implications for the impact of Northern Hemisphere cooling on ITCZ movement, *Earth Planet. Sci. Lett.*, *255*(1), 213–228.
Stoll, H. M., A. Arevalos, A. Burke, P. Ziveri, G. Mortyn, N. Shimizu, and D. Unger (2007b), Seasonal cycles in biogenic production and export in Northern Bay of Bengal sediment traps, *Deep Sea Res. Part II*, *54*(5), 558–580.
Sun, Y., S. C. Clemens, C. Morrill, X. Lin, X. Wang, and Z. An (2012), Influence of Atlantic meridional overturning circulation on the East Asian winter monsoon, *Nat. Geosci.*, *5*(1), 46–49.
Thompson, L. G., T. Yao, E. Mosley-Thompson, M. Davis, K. Henderson, and P.-N. Lin (2000), A high-resolution millennial record of the South Asian monsoon from Himalayan ice cores, *Science*, *289*(5486), 1916–1919.
Unger, D., V. Ittekkot, P. Schäfer, J. Tiemann, and S. Reschke (2003), Seasonality and interannual variability of particle fluxes to the deep Bay of Bengal: Influence of riverine input and oceanographic processes, *Deep Sea Res. Part II*, *50*(5), 897–923.
Vetter, L., H. J. Spero, A. D. Russell, and J. S. Fehrenbacher (2013), LA-ICP-MS depth profiling perspective on cleaning protocols for elemental analyses in planktic foraminifers, *Geochem. Geophys. Geosyst.*, *14*, 2916–2931, doi:10.1002/ggge.20163.

Wang, Y., H. Cheng, R. L. Edwards, X. Kong, X. Shao, S. Chen, J. Wu, X. Jiang, X. Wang, and Z. An (2008), Millennial-and orbital-scale changes in the East Asian monsoon over the past 224,000 years, *Nature*, *451*(7182), 1090–1093.

Wang, Y.-J., H. Cheng, R. L. Edwards, Z. An, J. Wu, C.-C. Shen, and J. A. Dorale (2001), A high-resolution absolute-dated late Pleistocene monsoon record from Hulu Cave, China, *Science*, *294*(5550), 2345–2348.

Webster, P. J. (1994), The role of hydrological processes in ocean-atmosphere interactions, *Rev. Geophys.*, *32*(4), 427–476.

Weldeab, S., D. W. Lea, R. R. Schneider, and N. Andersen (2007), 155,000 years of West African monsoon and ocean thermal evolution, *Science*, *316*(5829), 1303–1307. [11743199].

Zhang, R., and T. L. Delworth (2005), Simulated tropical response to a substantial weakening of the Atlantic thermohaline circulation, *J. Clim.*, *18*(12), 1853–1860.

Ziegler, M., L. J. Lourens, E. Tuenter, F. Hilgen, G.-J. Reichart, and N. Weber (2010), Precession phasing offset between Indian summer monsoon and Arabian Sea productivity linked to changes in Atlantic overturning circulation, *Paleoceanography*, *25*, PA3213, doi:10.1029/2009PA001884.